

Vortex Pinning and the Non-Hermitian Mott Transition

Raphael A. Lehrer and David R. Nelson

Lyman Laboratory of Physics, Harvard University, Cambridge, Massachusetts 02138

(January 28, 2018)

The boson Hubbard model has been extensively studied as a model of the zero temperature superfluid/insulator transition in ^4He on periodic substrates. It can also serve as a model for vortex lines in superconductors with a magnetic field parallel to a periodic array of columnar pins, due to a formal analogy between the vortex lines and the statistical mechanics of quantum bosons. When the magnetic field has a component perpendicular to the pins, this analogy yields a *non-Hermitian* boson Hubbard model. At integer filling, we find that for small transverse fields, the insulating phase is preserved, and the transverse field is exponentially screened away from the boundaries of the superconductor. At larger transverse fields, a “superfluid” phase of tilted, entangled vortices appears. The universality class of the transition is found to be that of vortex lines entering the Meissner phase at H_{c1} , with the additional feature that the direction of the tilted vortices at the transition bears a nontrivial relationship to the direction of the applied magnetic field. The properties of the Mott insulator and flux liquid phases with tilt are also discussed.

I. INTRODUCTION

The importance of interactions for vortex lines in superconductors has been well known since Abrikosov’s theory of the mixed phase of type II superconductors. The vortices form a regular triangular lattice due to their repulsive interactions. With the discovery of the cuprate high-temperature superconductors, however, it became clear that thermal fluctuations can play an important role in the behavior of the flux lines arrays. [1] The competition between interactions, pinning, and thermal fluctuations gives rise to a wide range of novel phenomena. For example, it is now clear that the triangular flux lattice melts via a first order transition [2] in clean materials, giving rise to an entangled flux liquid [3] over a significant part of the phase diagram.

Here we investigate the behavior of an interacting system of flux lines in a periodic array of columnar defects. Traditionally, columnar defects are made in high-temperature superconductors by heavy-ion bombardment. [4–8] The ions pass through the sample, leaving amorphous damage tracks in their wake, which act very effectively as pinning sites for the flux lines, provided the lines are aligned with the defects. Pinning is efficient in this case because the dimensions of the flux lines are comparable to those of the pins: both the vortices and the columnar defects are extended over the length of the sample in one direction, and the vortex core size ($\sim 20 \text{ \AA}$) is comparable to the width of the damage tracks ($\sim 60 \text{ \AA}$). By covering the sample with a mask with a periodic array of holes through which the ions can pass, a periodic array of pins (or clusters of pins) could be formed.

There are, however, other promising approaches to forming a periodic array of columnar defects in which the artificial pinning centers are able to accommodate multiple vortex lines per pin. Such structures have in fact already been made both in thick [9] and thin samples, [10] and one goal of this paper is to understand effects of thermal fluctuations and entanglement when the materials

are very thick. The work of Cooley *et al.* [9] is of particular interest to us, because their samples can potentially be used in two different ways to test our theories. Their samples have a regular lattice of pins within an “island.” The islands are themselves spaced periodically through the sample. We may use our theory to predict behavior of the pins within a single island; or, we may view each island as a large pinning center capable of accommodating many vortices and apply our theories to that as well. The lattices are triangular in either case. We here describe effects expected to be observed in square lattices of pinning sites; it is straightforward but tedious to generalize our results to triangular lattices as well.

Another motivation for examining flux lines in the presence of an ordered array of columnar pins is to better understand computer simulations such as those by Li and Teitel [11] and others [12] which attempt to model flux lines in cuprate superconductors. These authors use an underlying discretization (such as a stack of triangular lattices) for the simulations. Although layering along the c -axis is an important feature of real cuprates, the relatively coarse mesh of allowed sites for vortices in each layer is clearly an artifact of the simulations. As we shall see, the presence of such periodicity can cause significant changes (such as a transverse Meissner effect) in the behavior of the flux lines. The very existence of a periodic “Mott insulator” phase in these simulations (see below) with its massive phonon modes and infinite tilt modulus, is an artifact of the lattice discretization. In the absence of a lattice, the Mott insulator phase would be replaced by an Abrikosov crystalline phase with finite elastic constants. Our investigation can begin to delimit the circumstances under which lattice approximations fail as models of real materials, and to predict what kind of behavior might be observed when they do fail.

As a third motivation, we hope that studies such as this will lead to a better understanding of interacting flux lines with tilted field in a *random* array of columnar defects. [13,14] Although the extension of the stan-

standard theory of disordered superfluids to vortex lines with tilted magnetic fields is straightforward in principle [14,15] there are still poorly understood aspects of this problem.

To understand how our model differs from conventional lattice boson Hubbard models, [16] consider the transfer matrix generated by the classical partition function for wiggling vortex lines in $d + 1$ dimensions. This transfer matrix is the exponential of a d -dimensional non-Hermitian quantum Hubbard Hamiltonian [13,14]

$$\hat{H} = -t \sum_{\langle ij \rangle} \left(e^{\mathbf{h} \cdot \hat{\mathbf{e}}_{ij}} \hat{a}_j^\dagger \hat{a}_i + e^{-\mathbf{h} \cdot \hat{\mathbf{e}}_{ij}} \hat{a}_i^\dagger \hat{a}_j \right) - \mu \sum_j \hat{a}_j^\dagger \hat{a}_j + \frac{U}{2} \sum_j \hat{a}_j^\dagger \hat{a}_j \left(\hat{a}_j^\dagger \hat{a}_j - 1 \right). \quad (1.1)$$

The connection between this model and the physics of flux lines will be reviewed in more detail in Sec. II. Here, we simply note that the $\{\hat{a}_i^\dagger, \hat{a}_j\}$ are boson (i.e., vortex) creation and destruction operators, the $\hat{\mathbf{e}}_{ij}$ are unit vectors connecting nearest neighbor lattice sites on a square lattice representing the positions of columnar pins in d dimensions, and the first sum is over neighboring pairs of pins. The parameter t controls vortex hopping between columns, $\mu = \mu(H_z)$ is a chemical potential that depends on the component of the external field H_z parallel to the columns, and U represents the penalty for multiple vortices on a single defect. The external tipping field \mathbf{H}_\perp determines the non-Hermitian hopping asymmetry \mathbf{h} via $\mathbf{h} = \phi_0 \mathbf{H}_\perp a_0 / (4\pi k_B T)$, where a_0 is the lattice constant. In the presence of this non-Hermitian hopping, which would be impossible in conventional many body quantum mechanics, the excitation spectrum can become complex. The complex spectra which arise when $U = 0$ and μ varies randomly from site to site has aroused considerable interest recently. [14,17] In this paper, we study how this non-Hermiticity affects excitations and other features of the Mott insulator and superfluid phases.

Before discussing the interacting case, consider a system of *noninteracting* flux lines in the presence of a periodic array of columnar pins. At very low temperatures in thin samples, each vortex will be tightly bound to a particular pin, and fluctuations away from the pinning sites will be small. However, a flux line can gain entropy by hopping from one defect to another. For an infinitely thick sample, the vortices will in fact be delocalized at *any* nonzero temperature. In the quantum analogy, this delocalization is a consequence of the periodicity of the pinning potential and Bloch's theorem. [18] Although the distance in the $\hat{\mathbf{z}}$ -direction between intercolumn hops diverges as the temperature is lowered to zero, [19] we will assume sufficiently thick samples and high temperatures so that an individual vortex hops repeatedly as it traverses the sample. Such delocalized states are easy to tilt and will have a finite linear resistance, because transport in the presence of a Lorentz force will be aided by finite concentration of kinks in equilibrium. [13] Hopping

from one columnar pin to another *cannot* be neglected at finite temperatures in thick samples, even if such events are relatively rare.

We now discuss qualitatively the interacting case. Consider an external magnetic field H_z such that there is exactly one flux line per columnar pin, i.e., $B_z = \phi_0/a_0^2$. If the pins are strong enough, the ground state will be a square lattice of vortices rather than the usual triangular array that is observed in the absence of pins. Thermal fluctuations allow the lines to make short excursions away from the columnar pins which lowers the effective strength of the pins. [13] More substantive changes arise if thermal disorder also leads to hops from one pin to another, as for the noninteracting flux lines discussed above. However, the interactions inhibit hopping, due to the extra energy cost of double occupancy. [20] Although hopping increases the entropy per unit length, this is insufficient to overcome the energy barrier at low temperatures. Above a certain critical temperature T_c , however, the entropy gain dominates, and the flux lines can hop freely from pin to pin. In the quantum analogy, this phase change is the boson Mott transition [16] between a $2d$ Mott insulator (square vortex lattice) and a $2d$ superfluid (entangled vortex liquid). The temperature T for the vortices plays the role of \hbar for the bosons. (See Sec. II.)

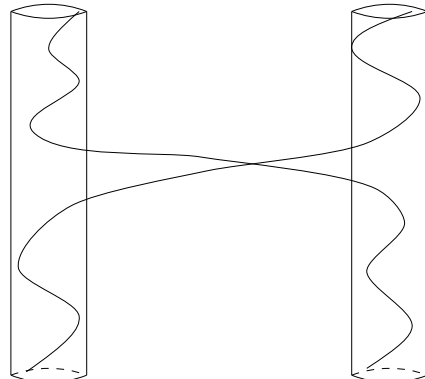


FIG. 1. An example of a correlated hopping event. Such hops delocalize flux lines, but cannot mediate vortex transport or tilt.

Correlated hopping events such as are shown in Fig. 1 can lower the entropy without forcing two flux lines to occupy the same column, and always delocalize lines in sufficiently thick samples even in the crystalline phase. However, such defects cannot mediate vortex transport or tilt—if one flux line moves to the right, another must move to the left, so there is no net change. Thus it will not be until the temperature rises above the critical temperature mentioned above that there will be any linear resistance or response to a perpendicular magnetic field.

Consider now raising the applied magnetic field $\mathbf{H} = H_z \hat{\mathbf{z}}$, always keeping it parallel to the column direction. In the absence of columnar pins, the lattice spacing would

simply shrink; however, if the pins are strong enough, a change in the lattice constant would sacrifice the energy benefit of commensurability with the lattice of pinning sites. An alternative response is the introduction of extra vortices into the commensurate lattice. Depending on the pinning strength, the additional vortices will either doubly occupy certain columnar pins, or else occupy interstitial sites; either possibility costs an extra energy cost per unit length. We assume for simplicity that the cost of double occupancy is lower [20], and call the resulting extra vortex a “particle” excitation. This “particle” has an energy per unit length of order the cost of double occupancy; however, it can gain entropy by hopping from pin to pin, and thus lower its *free energy*. In fact, its free energy can become negative. Following the treatment of interstitials and vacancies in a conventional Abrikosov lattice in Ref. [21], an estimate of the boundary above which particles are favored arises from approximating the partition function of a single extra vortex by $4^{L/l_z} \exp(-\epsilon_p L/T)$, where $\epsilon_p = \epsilon_p(H_z)$ is the energy cost per unit length of a particle, L is the length in the z direction, and l_z is the distance between hops of the particle from one site to another. If E_p is the extra energy of an particle in zero external magnetic field H , then $\epsilon_p(H) = E_p - \phi_0 H_z/4\pi$. The factor of 4 comes from the four directions available for hopping on a square lattice. Thus the free energy of the particle will be $F \approx \epsilon_p L - T(L/l_z) \ln 4$, which becomes negative above a temperature

$$T_d(H_z) = \frac{\epsilon_p(H_z)l_z}{\ln 4}. \quad (1.2)$$

Above this temperature, particles are favorable; below it, however, the system cannot respond to a change in H_z , and the extra magnetic field is screened out. Similar screening arises if one attempts to produce vacancies or “holes” by reducing the magnetic field, with $F_h \approx \epsilon_h L - T(L/l_z) \ln 4$, where ϵ_h is the hole energy in the absence of an external magnetic field. Thus for a range of applied fields H_z , the actual field B_z (as measured by the vortex density) will be locked in at the value $B_z = \phi_0/a^2$, much as in the Meissner effect where the field is locked in at $B = 0$ for a range of applied H_z . Similar arguments show that if we apply a small field \mathbf{H}_\perp transverse to the columns, isolated flux lines will not be able to tilt in response to it, and the field will again be screened out, i.e., $\mathbf{B}_\perp = \mathbf{0}$. [13]

In the rest of the paper, we examine the phase transitions described qualitatively above. The phase diagram is shown in Fig. 2. The “commensurate” Meissner-like phase discussed above for vortex matter is called a “Mott insulator” in the context of quantum bosons. With $\mathbf{H}_\perp = \mathbf{0}$, this problem has been studied by Fisher *et al.* [16] in the context of real quantum bosons on a lattice. In the presence of a transverse field, however, the formal analogy between the statistical mechanics of vortex matter and (2+1)-dimensional quantum mechanics leads to the *non-Hermitian* model of Eq. (1.1). [14]

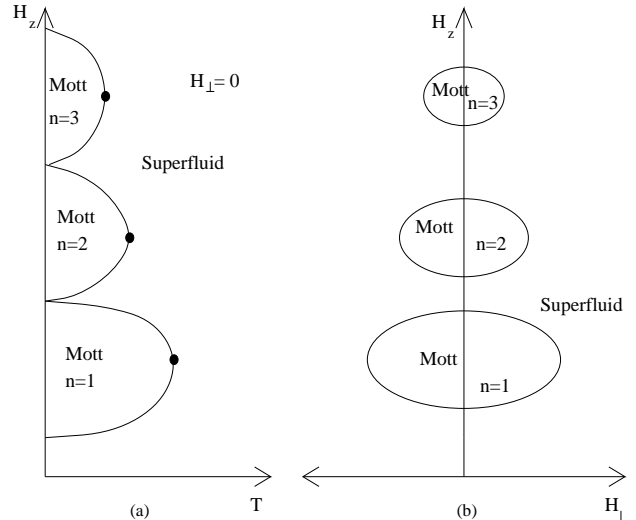


FIG. 2. (a) Schematic phase diagram for $\mathbf{H}_\perp = \mathbf{0}$. The circles at the tips of the Mott lobes are the multicritical points. (b) Schematic phase diagram at fixed temperature T below the multicritical points in (a).

In Sec. II, we describe in more detail our model of interacting vortex lines. We study the Mott insulator to flux liquid phase transition induced by a perpendicular field in Sec. III, using mean field theory and a more sophisticated renormalization group treatment. We argue that in the presence of a transverse field, the transition is characterized by the penetration of “tilted defects,” which are particles or holes with net average motion in response to the transverse field, as shown in Figs. 3 and 4. More support is given for this picture in Sec. IV, where the low temperature Mott insulator phase is examined. We determine excitation gaps for hopping in

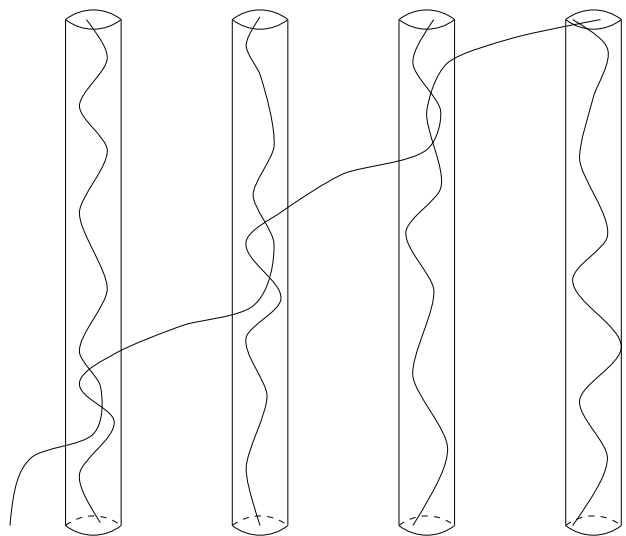


FIG. 3. An example of a right-moving tilted particle defect.

the presence of the non-Hermitian perturbation. We also calculate a quantity analogous to the London penetration depth in the Meissner phase, which is the length over which screening of the transverse magnetic field becomes effective near the boundaries over the sample. In Sec. V, we examine properties of the superfluid phase, particularly the way we expect the magnetic field to penetrate the sample near the transition, and the excitation spectrum.

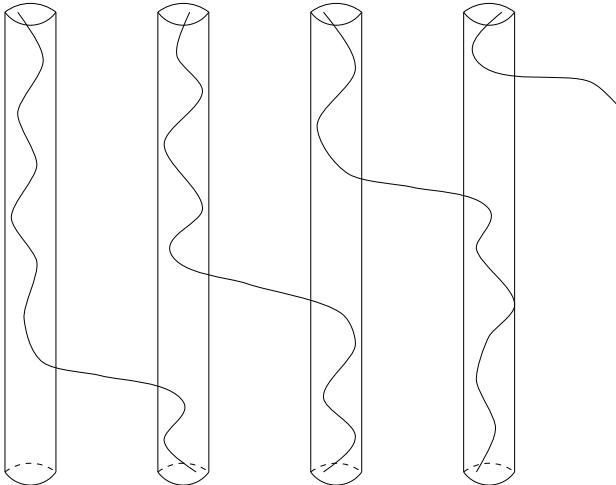


FIG. 4. An example of a right-moving tilted hole defect.

II. MODEL

We begin with a model free energy for N vortex lines in a sample of thickness L in the $\hat{\mathbf{z}}$ direction (perpendicular to the CuO_2 planes) in the presence of a periodic square array of columnar defects aligned in the $\hat{\mathbf{z}}$ direction with nearest neighbor separation a . We allow an external magnetic field \mathbf{H}_\perp transverse to the defects as well as the usual parallel field \mathbf{H}_\parallel . The energy then reads [13]

$$\begin{aligned}
 F_N = & \frac{1}{2} \tilde{\epsilon}_1 \sum_{\mu=1}^N \int_0^L \left| \frac{d\mathbf{r}_\mu(z)}{dz} \right|^2 dz \\
 & + \frac{1}{2} \sum_{\mu \neq \nu} \int_0^L V(|\mathbf{r}_\mu(z) - \mathbf{r}_\nu(z)|) dz \\
 & + \sum_{\mu=1}^N \int_0^L V_D[\mathbf{r}_\mu(z)] dz \\
 & - \frac{\mathbf{H}_\perp \phi_0}{4\pi} \cdot \sum_{\mu=1}^N \int_0^L \frac{d\mathbf{r}_\mu(z)}{dz} dz, \quad (2.1)
 \end{aligned}$$

with

$$V_D[\mathbf{r}_\mu(z)] = \sum_{i=1}^M V_1[|\mathbf{r}_\mu(z) - \mathbf{R}_i|]. \quad (2.2)$$

Greek letters denote the flux lines while Roman letters denote the columnar pins. $V(r)$ is the (repulsive) interaction potential between flux lines, which can be taken local in $\hat{\mathbf{z}}$, while V_1 describes the (attractive) interaction between a flux line and a columnar defect. The parameter $\tilde{\epsilon}_1$ in the kinetic energylike term arises from the tilt energy of the lines. This term is a quantitatively correct approximation to the tilt energy provided

$$\left| \frac{d\mathbf{r}_\mu(z)}{dz} \right|^2 \ll M_z/M_\perp, \quad (2.3)$$

where $M_z/M_\perp \gg 1$ is the mass anisotropy in the underlying Ginzburg-Landau theory. That same criterion insures that an interaction local in z is a good approximation. [13]

There is a useful formal correspondence between this flux line problem and fictitious quantum-mechanical bosons in two dimensions. [3,13]. The temperature T plays the role of Planck's constant \hbar , the bending energy $\tilde{\epsilon}_1$ plays the role of the boson mass m , and the length of the sample L corresponds to $\beta\hbar$ for the bosons. (See Table I for a summary.) However, while real bosons have *periodic* boundary conditions in imaginary time, *free* boundary conditions are more appropriate to the flux line system. As we take the thermodynamic limit $L \rightarrow \infty$ (corresponding to the zero temperature limit for the fictitious bosons), the partition function is dominated by the ground state, and the statistical mechanics is insensitive to the boundary conditions. Even for finite L , the only states which contribute to the partition function of the vortex lines are symmetrical boson states. [3] We defer consideration of finite size effects to Sec. IV B, while in the rest of this paper we use periodic boundary conditions for convenience and take the limit $L \rightarrow \infty$.

Vortex lines	Bosons
$\tilde{\epsilon}_1$	m
$k_B T$	\hbar
L_z	$\beta\hbar$
$H_z \phi_0 / 4\pi - \tilde{\epsilon}_1$	μ
$\mathbf{H}_\perp \phi_0 a_0 / 4\pi k_B T$	\mathbf{h}
Meissner-like commensurate phase	Mott insulator
Flux liquid	Superfluid

TABLE I. Detailed correspondence of the parameters of the flux line system with the parameters of the two-dimensional boson system.

As emphasized in Ref. [14], the transverse field \mathbf{H}_\perp plays the role of an *imaginary* vector potential in the boson system. Thus, understanding the flux line system in the presence of a transverse field is equivalent to understanding the quantum mechanics of *non-Hermitian* two-dimensional bosons with interactions and a periodic potential.

In the limit of a very strong columnar pinning potential, we can replace Eq. (2.1) by a simplified tight binding model for the vortex lines [13,14,20] such that, written in terms of the fictitious boson operators, the grand canonical partition function is

$$\mathcal{Z} = \text{Tr} \left\{ e^{-\beta L \hat{\mathcal{H}}} \right\}, \quad (2.4)$$

where $\hat{\mathcal{H}}$ given by Eq. (1.1) and L is the sample thickness. The non-Hermitian terms in the effective Hamiltonian reflect a preference for the bosons to hop in the direction of the transverse field. We have neglected interactions between flux lines that are not on the same site. This should give reasonable results near filling fraction 1; however, if we wanted to describe filling fraction 1/2, for example, where we might expect the ground state to be a checkerboard arrangement of the flux lines, we would need to include further neighbor interactions. Further neighbor interactions would also be required to treat the lattice models of melting studied numerically in Refs. [11] and [12].

The parameters of this model, expressed in the original flux line language are [13,14]

$$\mu = \frac{\mathbf{H}_z \phi_0}{4\pi} - \epsilon_1, \quad (2.5)$$

$$\mathbf{h} = \frac{\mathbf{H}_\perp \phi_0 a_0}{4\pi k_B T}, \quad (2.6)$$

$$U \approx 2\epsilon_0 \ln(H_{c2}/H), \quad (2.7)$$

$$t \approx 2 \left(\frac{2}{\pi} \right)^{1/2} \frac{V_0}{\sqrt{E_{ij}/T}} e^{-E_{ij}/T}, \quad (2.8)$$

with V_0 the strength of the pin and $E_{ij} = \sqrt{2\epsilon_1 V_0} a_0$ the WKB exponent for tunneling from one pin to its neighbor. The Hubbard U term in Eq. (1.1) contributes an energy $\frac{1}{2}Un(n-1)$ when n flux lines are on a single site. It represents the difference between the energy of a single n -fold vortex quantum ($\sim n^2$) and the energy of n well-separated unit vortices. In this tight-binding limit, a Mott insulator phase exists not only at filling fraction 1, but at any integer filling fraction. We will consider Mott insulator phases with general filling fraction n . Integer filling fraction with $n \geq 2$ would arise as an approximation to samples irradiated through a mask of holes large enough to allow multiple columnar defects at every lattice site.

III. TRANSITION AND RENORMALIZATION GROUP

Unless μ/U is exactly an integer [corresponding to the points where two Mott lobes are tangent in Fig. 2(a)], it is expected [16] that the equivalent quantum system will be in a Mott insulator phase with a well defined integer site occupation number n for sufficiently weak hopping

parameter t . As discussed in Sec. I, the ‘‘Mott insulator’’ corresponds to a Meissner-like vortex phase, which resists changes in the number of vortices per site. As is evident from Eq. (2.8), small t corresponds to low temperatures in the vortex system. Large hopping leads eventually to a 2nd order phase transition to a superfluid phase. This ‘‘superfluid’’ is a lattice analogue of an entangled flux liquid for vortex matter. In this section, we first mention a simple mean field theory due to Sheshadri, *et al.* [22] The detailed application of this mean field theory to the non-Hermitian boson Hubbard model is described in Appendix A. We then use a more systematic approach to study this transition which will allow us to determine the universality class of the transition. We defer a detailed discussion of the phases themselves until later sections.

A. Mean field theory

One simple way of accessing the mean field theory associated with Eq. (1.1) is with an ansatz that decouples the hopping term to give a single-site Hamiltonian via the replacement [22]

$$\hat{a}_i^\dagger \hat{a}_j \rightarrow \langle \hat{a}_i^\dagger \rangle \hat{a}_j + \hat{a}_i^\dagger \langle \hat{a}_j \rangle - \langle \hat{a}_i^\dagger \rangle \langle \hat{a}_j \rangle. \quad (3.1)$$

In the remainder of this section, however, we follow a different approach that allows a more convenient treatment of fluctuation effects. The decoupling method, however, is conceptually and computationally simpler, so we present it in Appendix A.

B. Hubbard-Stratanovich transformation

We here transform the tight binding partition function of Eq. (2.4) and Eq. (1.1) into a field theoretic form more convenient for calculation following a method used by Fisher, *et al.* [16], and earlier by Doniach [23], to treat a quantum model of coupled arrays of Josephson junctions. We begin by separating the Hamiltonian $\hat{\mathcal{H}}_N$ of Eq. (1.1) into the single site piece $\hat{\mathcal{H}}_0$ and the off-site hopping term $\hat{\mathcal{H}}_1$: $\hat{\mathcal{H}} = \hat{\mathcal{H}}_0 + \hat{\mathcal{H}}_1$, with

$$\hat{\mathcal{H}}_0 = \sum_i \left[\frac{U}{2} \hat{n}_i (\hat{n}_i - 1) - \mu \hat{n}_i \right], \quad (3.2)$$

$$\hat{\mathcal{H}}_1 = -\frac{1}{2} \sum_{i,j} [J_{ij} \hat{a}_i^\dagger \hat{a}_j + J_{ji} \hat{a}_j^\dagger \hat{a}_i], \quad (3.3)$$

where $\hat{n}_i = \hat{a}_i^\dagger \hat{a}_i$ is the number operator and J_{ij} is the hopping matrix element between sites i and j :

$$J_{ij} = \begin{cases} t e^{\mathbf{h} \cdot \hat{\mathbf{e}}_{ij}} & \text{if } i, j \text{ nearest neighbors} \\ 0 & \text{otherwise.} \end{cases} \quad (3.4)$$

The generalization of the transformations of Refs. [23] and [16] to the non-Hermitian case presents no difficulties. Their effect is to allow the grand canonical partition

function of Eq. (2.4) to be rewritten as a functional integral over a set of complex functions $\{\psi_i(\tau)\}$,

$$\mathcal{Z} = \mathcal{Z}_0 \int \prod_i \mathcal{D}\psi_i(\tau) \mathcal{D}\psi_i^*(\tau) \exp[-S(\psi)], \quad (3.5)$$

with an effective action

$$S(\psi) = \beta \sum_{i,j} \int_0^L d\tau (J^{-1})_{ij} \psi_i^*(\tau) \psi_j(\tau) - \sum_i \ln \left\langle T_\tau \exp \left[\beta \int_0^L d\tau \{ \psi_i(\tau) \hat{a}_i^\dagger(\tau) + \psi_i^*(\tau) \hat{a}_i(\tau) \} \right] \right\rangle_0, \quad (3.6)$$

where T_τ is the imaginary-time ordering operator,

$$\mathcal{Z}_0 = \text{Tr} \left\{ e^{-\beta L \hat{H}_0} \right\}, \quad (3.7)$$

$$\langle \bullet \rangle_0 = \frac{1}{\mathcal{Z}_0} \text{Tr} \left\{ e^{-\beta L \hat{H}_0} \bullet \right\}, \quad (3.8)$$

and the imaginary time dependence of operators is given by, e.g.,

$$\hat{a}_i(\tau) = e^{\beta\tau \hat{H}_0} \hat{a}_i e^{-\beta\tau \hat{H}_0}. \quad (3.9)$$

We can see the equivalence of Eq. (3.5) with Eq. (2.4) by integrating out the ψ fields to obtain

$$\mathcal{Z} = \mathcal{Z}_0 \left\langle T_\tau \exp \left[-\beta \int_0^L d\tau \hat{\mathcal{H}}_1(\tau) \right] \right\rangle_0, \quad (3.10)$$

which is just the familiar interaction representation of Eq. (2.4).

C. Universality classes

Since $\langle \psi_i \rangle$ is an order parameter for superfluidity [23,16] we can study the transition to a state with $\langle \psi_i \rangle \neq 0$ by expanding Eq. (3.6) in powers of ψ . For now, we keep only the most relevant terms in a long-wavelength approximation, and obtain

$$S(\psi) \approx \beta a_0^2 \int \frac{d^2 \mathbf{k} d\omega}{(2\pi)^3} |\psi(\mathbf{k}, \omega)|^2 [r - ic_\mu \omega + i \mathbf{c}_h \cdot \mathbf{k} + c' \omega^2 + D_{ij} k_i k_j] + u \int d^2 \mathbf{r} d\tau |\psi(\mathbf{r}, \tau)|^4, \quad (3.11)$$

as shown in Appendix B. This formula is applicable to a Mott insulator phase with n particles per site (i.e. $n-1 < \mu/U < n$). The values of the parameters $r(\mu, T)$, c' , u , and the matrix D_{ij} are given in Appendix B, while

$$c_\mu = k_B T \left(\frac{n+1}{E_p^2} - \frac{n}{E_h^2} \right), \quad (3.12)$$

$$\mathbf{c}_h = \frac{a_0}{2t} \frac{\hat{\mathbf{x}} \sinh h_x + \hat{\mathbf{y}} \sinh h_y}{[\cosh h_x + \cosh h_y]^2}, \quad (3.13)$$

where

$$E_p = Un - \mu, \quad (3.14)$$

$$E_h = \mu - U(n-1) \quad (3.15)$$

are (respectively) the energies of ‘‘particles’’ and ‘‘holes’’ superimposed on a Mott insulator state with a fixed value of n , in the absence of hopping.

Note that c_μ and \mathbf{c}_h can be positive, negative, or zero. In the case examined in Fisher *et al.*, there is no transverse field, i.e., $\mathbf{c}_h = 0$. If $c_\mu = 0$ as well, then the universality class of the transition which occurs for $r \approx 0$ is that of the XY model in three dimensions, with nontrivial critical exponents due to fluctuations. When $c_\mu > 0$, the transition at $r \approx 0$ is characterized instead by mean field exponents with logarithmic corrections. [16,24] This is also the universality class which describes the penetration of thermally excited vortex lines from the Meissner phase near H_{c1} . [3] Near this transition, extra vortex lines enter into the sample and behave (at long length scales) like a dilute gas of weakly interacting bosons. When $c_\mu < 0$, the universality class is again like flux penetration near H_{c1} , with the magnetic field reversed. Now, holes enter the sample and behave (at long wavelengths) like a dilute system of linelike excitations in the negative $\hat{\mathbf{z}}$ direction.

When a transverse field is applied, $\mathbf{c}_h \neq 0$, and we see from Eq. (3.11) that the transition again resembles the physics of dilute linelike excitations near H_{c1} , but in a direction given by the three dimensional vector

$$\mathbf{v} = \mathbf{c}_h + c_\mu \hat{\mathbf{z}}. \quad (3.16)$$

When $r(\mu, T) \lesssim 0$, tilted holes or extra vortices enter the sample, at an angle determined by Eq. (3.16). See Figs. 3 and 4 for illustrations of tilted particle and hole defects, and see Fig. 5 for the range of parameter space in which we expect each type of defect. The renormalization group calculation that describes the transition, including effects of the underlying square columnar lattice of preferred sites, is given in Appendix C.

We confirm this interpretation of the physics when we examine the Mott insulator and superfluid phases in Secs. IV and V. In the Mott insulator, we calculate the energies per unit length of defects constrained to have a specific average direction, and find that only those oriented in direction $\hat{\mathbf{v}}$ have vanishing energies per unit length as we approach the transition. Thus, near the transition, only defects in this specific orientation will have favorable energy and proliferate. In the superfluid phase, we calculate the magnetic field change $\delta \mathbf{B}$ in excess of the field \mathbf{B}_0 locked into the Mott insulator phase, and find that it lies in the $\hat{\mathbf{v}}$ direction as well, corroborating our assertion that the defects penetrate at an average angle

$$\theta_v = \tan^{-1} \left(\frac{|\mathbf{c}_h|}{c_\mu} \right), \quad (3.17)$$

$$\phi_v = \tan^{-1} \left(\frac{c_{h_y}}{c_{h_x}} \right), \quad (3.18)$$

where θ_v and ϕ_v are polar angles with respect to the $\hat{\mathbf{z}}$ axis.

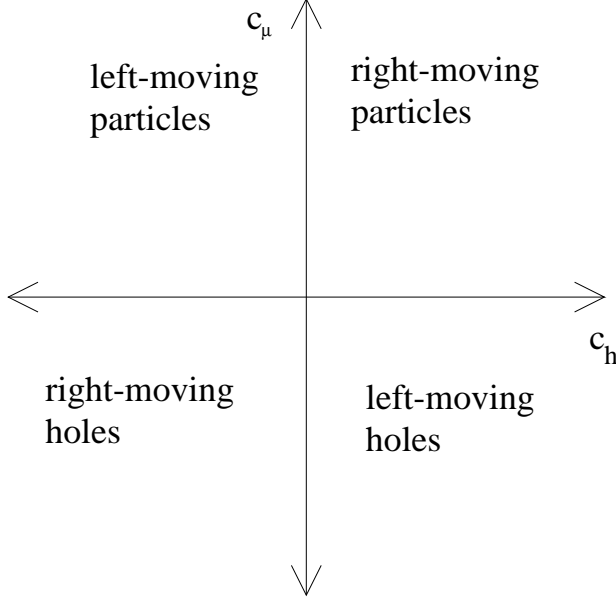


FIG. 5. The range of parameter space in which we expect to see various kinds of defects as we cross to the superfluid side of the Mott insulator/superfluid transition. The parameters c_μ and \mathbf{c}_h are defined in Eqs. (3.12) and (3.13).

D. Relationship between defect angle and the direction of the applied magnetic field

Note that these angles are not the same as the direction of the excess applied field, defined to be the additional field beyond that which produces the Mott insulator background. We denote this excess field by $\delta\mathbf{H} \equiv \mathbf{H} - H_0\hat{\mathbf{z}}$. Because there is actually a *range* of fields that produce the Mott insulator phase (see Fig. 2), we define H_0 so that $c_\mu = 0$ when $\delta H_z = 0$. Then a comparison of the direction of the defects with the direction of $\delta\mathbf{H}$ near the transition $r = 0$ gives

$$\tan \phi_v = \frac{\sinh h_y}{\sinh h_x}, \quad (3.19)$$

$$\tan \phi_{\mathbf{H}} = \frac{h_y}{h_x} \quad (3.20)$$

for the azimuthal angles, and

$$\tan \theta_v = \frac{a_0 t (U + \mu)}{k_B T \Delta \mu_0} \sqrt{\sinh^2 h_x + \sinh^2 h_y}, \quad (3.21)$$

$$\tan \theta_{\mathbf{H}} = \frac{k_B T |\mathbf{h}|}{a_0 \Delta \mu_0} \quad (3.22)$$

for the polar angles, where

$$\Delta \mu_0 = \frac{1}{2} [E_h - E_p + 2t(\cosh h_x + \cosh h_y)] \quad (3.23)$$

$$\equiv \mu - \mu_0, \quad (3.24)$$

with

$$\mu_0 = U(n - 1/2) - t(\cosh h_x + \cosh h_y). \quad (3.25)$$

From the equations for the azimuthal angles, we can see that the defects will tend to penetrate along the crystallographic axes defined by the square lattice of columnar defects. This is because the kink energy is smaller for hopping along the nearest neighbor directions, and is further emphasized by Fig. 6, which shows the relationship between ϕ_v and $\phi_{\mathbf{H}}$. To better compare θ_v and $\theta_{\mathbf{H}}$, we note that at the transition, we can write the ratio

$$\frac{\tan \theta_v}{\tan \theta_{\mathbf{H}}} = \frac{a_0^2 t U}{(k_B T)^2} f(\mu, \mathbf{h}), \quad (3.26)$$

where

$$f(\mu, \mathbf{h}) = \left(1 + \frac{\mu}{U} \right) \frac{\sqrt{\sinh^2 h_x + \sinh^2 h_y}}{|\mathbf{h}|}, \quad (3.27)$$

and μ and \mathbf{h} are related by the constraint that we are at the transition $r = 0$. The prefactor $a_0^2 t U / (k_B T)^2$ gives the order of magnitude of the ratio of $\tan \theta_v$ to $\tan \theta_{\mathbf{H}}$, as the (dimensionless) function $f(\mu, \mathbf{h})$ is of order 1 unless $|\mathbf{h}| \gg 1$.

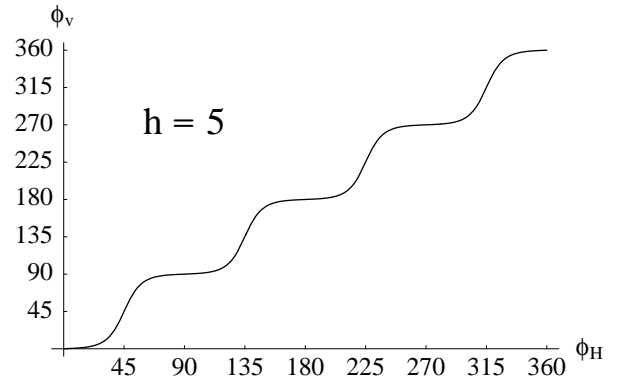


FIG. 6. A plot of the azimuthal angle of the average direction of defects versus the azimuthal angle of the excess applied field, for a fixed $|\mathbf{H}_\perp|$.

E. Scaling analysis near the multicritical point

A formal scaling analysis determines the shape of the transition line near the multicritical XY transition. Generalized to $\mathbf{c}_h \neq 0$, the scaling form [16] for the singular part of the free energy f_s near the multicritical point $c = \mathbf{c}_h = 0, \delta \equiv r - r_c = 0$ reads

$$f_s(\delta, \mathbf{c}_h, c) \sim b^{-d} f_s(\delta b^{1/\nu_{XY}}, \mathbf{c}_h b^{\lambda_h}, c_\mu b^{\lambda_\mu}) \quad (3.28)$$

for a length rescaling parameter b . λ_h and λ_μ are the renormalization group eigenvalues for \mathbf{c}_h and c_μ respectively. Although the scaling prefactor is $b^{-(d-1)-z}$ in general, we use the fact that $z = 1$ near the XY transition.

If we choose b such that $|\delta| b^{1/\nu_{XY}} = 1$, we obtain

$$f_s(\delta, \mathbf{c}_h, c_\mu) \sim |\delta|^{d\nu_{XY}} \Phi_\pm(\mathbf{c}_h |\delta|^{-\nu_{XY} \lambda_h}, c_\mu |\delta|^{-\nu_{XY} \lambda_\mu}), \quad (3.29)$$

where $\Phi_\pm(\mathbf{x}, z)$ is a scaling function that depends on whether $\delta > 0$ or $\delta < 0$.

A straightforward generalization of arguments in Ref. [16] yields $\lambda_h = \lambda_\mu = 1$ and Eq. (3.29) becomes

$$f_s(\delta, \mathbf{c}_h, c_\mu) \sim |\delta|^{d\nu_{XY}} \Phi_\pm(\mathbf{c}_h |\delta|^{-\nu_{XY}}, c_\mu |\delta|^{-\nu_{XY}}). \quad (3.30)$$

The function $\Phi_-(\mathbf{x}, z)$ is singular along a curve $[\mathbf{x}_c(z), z]$, which is necessary to describe the superfluid/Mott insulator transition away from the special multicritical point at $c_\mu = \mathbf{c}_h = 0$. Thus $\mathbf{c}_h \sim c_\mu \sim |\delta|^{\nu_{XY}}$ on the transition line. Since $\nu_{XY} < 1$ in three dimensions, there is no cusp in the phase diagram, in contrast to the Bose Glass phase. [13]

IV. MOTT INSULATOR PHASE

The renormalization group analysis described in Appendix C allows us to relate quantities near the transition to quantities deep within the Mott insulator or superfluid phases. The Mott insulator is characterized by the energy gaps for excitations. The magnitude of these gaps will control transport properties of the sample, as exemplified in Sec. IV A 3 where we calculate the nonlinear resistivity in the Mott insulator phase.

We can study these gaps far from the transition by expanding Eq. (3.6) to lowest order in ψ , keeping all terms quadratic in ψ , not just the most relevant in a small \mathbf{k} and ω expansion. As shown in Appendix B,

$$S(\psi) \approx S_0(\psi) = \beta a_0^2 \int \frac{d^2 \mathbf{k} d\omega}{(2\pi)^3} |\psi(\mathbf{k}, \omega)|^2 \times \left[\widetilde{J}^{-1}(\mathbf{k}) - \frac{n}{E_h + i\omega k_B T} - \frac{n+1}{E_p - i\omega k_B T} \right]. \quad (4.1)$$

Here $(\widetilde{J}^{-1})(\mathbf{k})$ is the Fourier transform of $(J^{-1})_{ij}$, given by

$$\widetilde{J}^{-1}(\mathbf{k}) = \frac{1}{2t} \frac{1}{\cos(k_x a_0 + ih_x) + \cos(k_y a_0 + ih_y)} \quad (4.2)$$

for a square lattice of columnar pinning sites, and E_p and E_h are defined by Eqs. (3.14) and (3.15). The particle energy E_p is the energy arising from Eq. (1.1) of a ‘‘frozen’’ extra vortex, i.e., with no contribution from the entropy gain due to wandering of the particle. In the quantum analogy, this entropy is represented by zero point motion. Similarly, E_h is the hole energy associated with a missing vortex frozen at a single site of a Mott insulator state with n vortices per site.

We remark that the quadratic expansion in ψ is sufficient to determine the Mott insulator/superfluid phase boundary within mean field theory. The Mott insulator phase is stable provided the coefficient of the $|\psi(\mathbf{k}, \omega)|^2$ term is positive for all \mathbf{k} and ω . Thus the mean field transition is determined by the first mode that vanishes, which is the $\mathbf{k} = \mathbf{0}, \omega = 0$ mode. Therefore, the transition occurs at $r(\mu, \mathbf{H}_\perp, T) = 0$, where r , the parameter given in Eq. (3.11), is given by

$$r = \frac{1}{2t} \frac{1}{\cosh h_x + \cosh h_y} - \frac{n}{E_h} - \frac{n+1}{E_p}. \quad (4.3)$$

The decoupling method also leads to a transition at $r = 0$, as shown in Appendix A.

A. Energy gaps for particles and holes

Because quantities deep in the Mott insulator phase are well described by Gaussian fluctuations, we focus on the quadratic approximation, and describe later how the results change close to the Mott insulator/superfluid transition.

1. Gaussian fluctuation effects

To determine the free energy cost per unit length of adding a particle or a hole to the Mott insulator phase, we show that

$$G(\tau) = \langle \psi(\mathbf{r}, \tau) \psi^*(\mathbf{r}, 0) \rangle \quad (4.4)$$

$$\sim \begin{cases} e^{-F_p \tau / k_B T} & \text{for } \tau > 0 \\ e^{-F_h |\tau| / k_B T} & \text{for } \tau < 0 \end{cases} \quad (4.5)$$

in the $\tau \rightarrow \infty$ limit. This Green’s function describes an extra vortex line created and destroyed at position \mathbf{r} for a time τ when τ is positive. For $\tau < 0$, it represents a hole. We identify F_p with the (free) energy cost per unit length of a particle and F_h with the (free) energy cost per unit length of a hole in the Mott insulator. These energies will be lower than the energy per unit length of particles or holes localized to a single site (E_p and E_h), because they can gain entropy from wandering and hence lower

their free energies. [21] In the quantum analogy, these energies are the “gaps” associated with particle and hole excitations in the Mott insulator phase.

The Hubbard-Stratanovich transformed action of Eq. (4.1) immediately yields

$$G(\tau) = \int \frac{d^2k}{(2\pi)^2} G(\mathbf{k}, \tau), \quad (4.6)$$

with

$$G(\mathbf{k}, \tau) = \frac{1}{\beta a_0^2} \int_{-\infty}^{\infty} \frac{d\omega}{2\pi} \frac{e^{-i\omega\tau}}{\widetilde{J}^{-1}(\mathbf{k}) - \frac{n}{E_h + i\omega k_B T} - \frac{n+1}{E_p - i\omega k_B T}}. \quad (4.7)$$

For $r > 0$, i.e., in the Mott insulator phase, the integrand has *two* poles, one each in the upper half and lower half of the complex- ω plane. Thus *both* particles and holes are represented by the single complex field ψ . This is to be contrasted with the situation usually encountered in vortex physics, e.g. the one considered in Ref. [3], where the coherent state complex field represents only one type of defect (vortex lines).

Upon solving for the location of the poles and then carrying out the momentum integrals by steepest descents in the limit $|\tau| \rightarrow \infty$, we find that the defect free energies are

$$F_{p,h} = \left\{ (\Delta\mu_1)^2 + E_p E_h \left[4rt + 2 \frac{\sinh^2(h_x/2) + \sinh^2(h_y/2)}{\cosh h_x + \cosh h_y} \right] \right\}^{1/2} \mp \Delta\mu_1, \quad (4.8)$$

where the upper sign applies to particles and the lower to holes, with

$$\Delta\mu_1 = \frac{1}{2}(E_h - E_p + 4t) \quad (4.9)$$

$$\equiv \mu - \mu_1, \quad (4.10)$$

and

$$\mu_1 = U(n - 1/2) - 2t. \quad (4.11)$$

When $\mu > \mu_1$, particles are preferred over holes, while for $\mu < \mu_1$, holes are preferred. If we set $\mu = \mu_1$, particle/hole symmetry is restored. When $\mathbf{h} = \mathbf{H}_\perp = \mathbf{0}$, then as we approach the Mott insulator/superfluid transition ($r \rightarrow 0^+$) along a generic path with $\mu \neq \mu_1$, the energy of the preferred defect vanishes like r , while the remaining defect energy remains finite as $r \rightarrow 0$. When $\mu = \mu_1$, however, both defect energies vanish simultaneously proportional to \sqrt{r} .

If we restore a transverse field, i.e. take $\mathbf{h} \neq \mathbf{0}$, then *neither* the particle nor the hole free energies defined by Eq. (4.8) vanish as $r \rightarrow 0$. However, as discussed in Sec. III C and illustrated in Fig. 5, we expect that *tilted*

particles or holes proliferate at the transition at a nonzero angle relative to the $\hat{\mathbf{z}}$ axis. To see that the corresponding defect energy vanishes at the transition, consider

$$G(l, \theta, \phi) = \langle \psi(\mathbf{r}, \tau) \psi^*(\mathbf{0}, 0) \rangle \quad (4.12)$$

$$= \int \frac{d^2k d\omega}{(2\pi)^3} e^{i(k_x x + k_y y - \omega\tau)} G(\mathbf{k}, \omega) \quad (4.13)$$

$$\sim \exp[-F(\theta, \phi)l/k_B T], \quad (4.14)$$

where we parametrize the transverse and τ -axis separations embodied in Eq. (4.12) as

$$\mathbf{r} = (l \sin \theta \cos \phi, l \sin \theta \sin \phi), \quad (4.15)$$

$$\tau = l \cos \theta, \quad (4.16)$$

and we eventually take the $l \rightarrow \infty$ limit.

To carry out this Fourier transform, we rotate to a new coordinate frame (\mathbf{k}', ω') , with

$$\omega' = \omega \cos \theta - k_x \sin \theta \cos \phi - k_y \sin \theta \sin \phi \quad (4.17)$$

so that

$$G(l, \theta, \phi) = \int \frac{d^2k' d\omega'}{(2\pi)^3} e^{-i\omega' l} G(\mathbf{k}', \omega'). \quad (4.18)$$

We note that the ω' integral will be dominated in the $l \rightarrow \infty$ limit by the closest singularity ω^* of $G(\mathbf{k}, \omega)$ to the real axis in the lower half of the complex frequency plane, and will behave as $\exp[-F(\mathbf{k}', \theta, \phi)l/k_B T]$, where

$$F(\mathbf{k}', \theta, \phi) = i\omega^* k_B T. \quad (4.19)$$

The \mathbf{k}' integrals are done by steepest descents, so

$$G(l, \theta, \phi) \sim e^{-F(\mathbf{k}'_*, \theta, \phi)l/k_B T}, \quad (4.20)$$

where \mathbf{k}'_* is chosen such that $\partial F(\mathbf{k}', \theta, \phi)/\partial \mathbf{k}'|_{\mathbf{k}'_*} = 0$. $F(\theta, \phi)$ can be found numerically for any θ, ϕ , but the low energy excitations can be found quite simply. We look for solutions which obey

$$F(\theta, \phi) \rightarrow 0 \text{ as } r \rightarrow 0^+. \quad (4.21)$$

In other words, the lower-half plane pole of the Green's function should vanish as we approach the transition. But $G^{-1}(\mathbf{k}' = 0, \omega' = 0) = 0$ at the transition, and indeed this is the only mode to vanish for $r \geq 0$. Thus we conclude that if (θ, ϕ) is chosen appropriately to provide a low energy excitation, then $\mathbf{k}'_* = 0$.

The angle that satisfies this condition is therefore defined by

$$\left. \frac{\partial F(\mathbf{k}', \theta, \phi)}{\partial \mathbf{k}'} \right|_{\mathbf{k}'=0} = 0. \quad (4.22)$$

Hence, in a small wavelength expansion of $G^{-1}(\mathbf{k}', \omega')$, there must be no terms linear in \mathbf{k}' . But notice that in the $(\tilde{\mathbf{k}}, \tilde{\omega})$ frame of Appendix C, the action has no terms linear in $\tilde{\mathbf{k}}$. Therefore, $(\tilde{\mathbf{k}}, \tilde{\omega}) = (\mathbf{k}', \omega')$, and the angles

(θ, ϕ) at which there are low energy excitations are exactly those in Eqs. (3.17) and (3.18). As expected, the direction in which there are low energy excitations is the same as the average direction of the defects in the superfluid phase.

To find the energy of these excitations, we need to find the poles of the Green's function at $\mathbf{k}' = 0$ and small ω . From Eq. (C1), we immediately see that the pole of interest is at $i\omega' = r/|\mathbf{v}|$, so

$$F(\theta, \phi) = \frac{r}{|\mathbf{v}|} \quad (4.23)$$

in the $r \rightarrow 0^+$ limit.

This analysis is clearly valid away from the multicritical point $\mathbf{v} = 0$. If $\mathbf{v} = 0$, then $\partial F(\mathbf{k}', \theta, \phi)/\partial \mathbf{k}'|_{\mathbf{k}'=0} = 0$ for all θ and ϕ , so there are low energy excitations at *all* angles. It is then clear from Eq. (3.11) that, at the level of Gaussian fluctuations,

$$F(\theta, \phi) \sim \sqrt{r} \quad (4.24)$$

for all θ and ϕ as $r \rightarrow 0^+$, with the coefficient depending on the angle.

2. Defect free energy at the XY transition

While we expect the Gaussian fluctuation analysis to be valid (up to logarithmic corrections) near the generic transition, there will be nontrivial corrections near the XY transition at the multicritical point $c_\mu = 0$, $\mathbf{c}_h = 0$. Close to this special point, we find that the free energy F_{XY} of defect lines at all angles scales in the same way with r within the Gaussian fluctuation analysis

$$F_{XY} \sim \sqrt{r} \sim \xi_{XY}^{-1/2}, \quad (4.25)$$

where $\xi_{XY} \sim 1/r$ is the Gaussian or mean field theory correlation length. To incorporate the effects of thermal fluctuations near the transition, we note that F_{XY} is actually an inverse correlation length in the imaginary time direction. Because the dynamic scaling exponent near the special multicritical XY transition is $z = 1$, we expect

$$F_{XY} \sim (r - r_c)^{\nu_{XY}}, \quad (4.26)$$

where $\nu_{XY} \approx 2/3$ is the correlation length exponent of the three-dimensional XY model, and r_c is the transition point renormalized by fluctuations. Equation (4.26) is, of course, the behavior predicted for the energy gap near the transition predicted by Fisher *et al.* [16]

3. Nonlinear resistivity in the Mott insulator phase

We now determine the form of the nonlinear current-voltage characteristics for a current perpendicular to the

vortex lines in the Mott insulator phase. Although the linear resistivity vanishes, supercurrents in the (x, y) -plane generate a nonzero voltage due to thermally activated nucleation and growth of particle-hole pairs. To calculate this resistivity, we estimate the free energy of a particle-hole pair of a given size in the presence of an externally imposed current \mathbf{J} . We expect that on scales much larger than a_0 , the lowest energy configuration will be approximately given by a loop (see Fig. 7). Then, following the analysis of Fisher, Fisher, and Huse for a conventional Meissner phase, [25] we estimate the free energy of a loop of radius $R \gg a_0$ lying in a plane normal to the current to be

$$F_{\text{loop}} \approx 2\pi R \bar{F} - J \frac{\phi_0}{c} \pi R^2, \quad (4.27)$$

where the second term arises from work done against the Lorentz force and the first is the line free energy of the loop. If \mathbf{J} is in the $(\theta_J = \pi/2, \phi_J)$ direction, then the average energy per unit length of the particle-hole pair is

$$\bar{F} = \frac{1}{\pi} \int_0^\pi \left[F\left(\theta, \phi_J - \frac{\pi}{2}\right) + F\left(\theta, \phi_J + \frac{\pi}{2}\right) \right] d\theta, \quad (4.28)$$

as illustrated in Fig. 7.

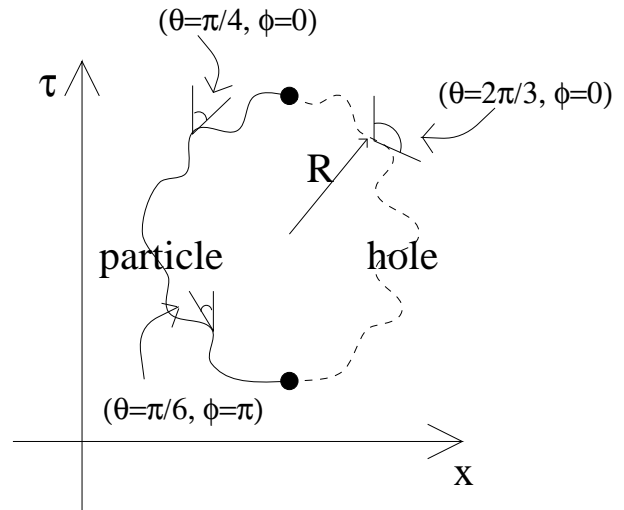


FIG. 7. A particle/hole defect loop which gives rise to a nonlinear resistivity by nucleating and growing in response to a current perpendicular to the (x, τ) plane.

F_{loop} has a maximum at $R_c \approx c\bar{F}/J\phi_0$, yielding a free energy barrier of approximately $\pi c\bar{F}^2/J\phi_0$. Thus the voltage generated by loops going over the barrier takes the form

$$V \sim e^{-J_T/J}, \quad (4.29)$$

with

$$J_T \approx \frac{\pi c \bar{F}^2}{\phi_0 T}. \quad (4.30)$$

We expect this to be valid for

$$J \ll \frac{c\bar{F}}{\phi_0 a_0}. \quad (4.31)$$

Therefore, near the XY transition, we find from Eq. (4.26) that

$$J_T \sim (r - r_c)^{2\nu_{XY}}. \quad (4.32)$$

Near the generic transition, J_T does not vanish, but instead approaches a nonzero constant. The exact value of \bar{F} is tedious to obtain, but it can be estimated as $\bar{F} \approx \frac{1}{2}(F_p + F_h)$, or

$$\bar{F} \approx \left\{ (\Delta\mu_1)^2 + E_p E_h \left[4rt + 2 \frac{\sinh^2(h_x/2) + \sinh^2(h_y/2)}{\cosh h_x + \cosh h_y} \right] \right\}^{1/2}, \quad (4.33)$$

where $\Delta\mu_1$ is given in Eq. (4.9).

B. Finite size effects in the Mott insulator

In this section, we discuss the difference between the periodic boundary conditions appropriate to real quantum bosons and the free boundary conditions appropriate to flux lines. In the Mott insulator phase, the transverse magnetic field is screened in the bulk of the sample where the vortices are localized on lattice sites, a phenomenon known as the transverse Meissner effect. [13] However, near the boundaries of the sample along the τ -direction, the transverse field will be able to penetrate. We show here that surface effects fall off exponentially with distance and calculate the corresponding screening length. This length scale plays a role similar to the usual London penetration depth in the Meissner phase, but is physically distinct, as it arises from the existence of a periodic pinning potential.

It is convenient to characterize surface effects by $\langle \hat{\mathcal{H}}_1 \rangle_\tau$, where $\langle \hat{\mathcal{H}}_1 \rangle_\tau$ is the matrix element of Eq. (3.3) in the Heisenberg representation,

$$\langle \hat{\mathcal{H}}_1 \rangle_\tau = \langle \psi_f | e^{-\beta(L-\tau)\hat{\mathcal{H}}} \hat{\mathcal{H}}_1 e^{-\beta\tau\hat{\mathcal{H}}} | \psi_i \rangle, \quad (4.34)$$

and $|\psi_i\rangle$ and $|\psi_f\rangle$ are initial and final boson states appropriate to “free” boundary conditions. By “free” boundary conditions, we mean that one integrates freely over the positions at which vortices enter and exit the sample. As discussed in Ref. [3], this boundary condition can be represented in the boson mapping by

$$|\psi_i\rangle = |\psi_f\rangle = e^{\sqrt{n_0}} |0\rangle, \quad (4.35)$$

where $n_0 = \sum_j \hat{a}_j^\dagger \hat{a}_j$ and $|0\rangle$ is the vacuum state.

Recall $\hat{\mathcal{H}}_1$ is the hopping term, which leads to a free energy reduction due to the wandering of the flux lines.

Because vortex fluctuations are less constrained near a free surface, we expect that $\hat{\mathcal{H}}_1$ exceeds its bulk value near the surface $\tau = 0$. In Appendix D, we show more precisely that

$$\langle \hat{\mathcal{H}}_1 \rangle_\tau - \langle \hat{\mathcal{H}}_1 \rangle_{\tau=\infty} \sim e^{-\tau/\tau^*} \quad (4.36)$$

as $\tau \rightarrow \infty$, with

$$\tau^* = \frac{k_B T}{F_p + F_h}, \quad (4.37)$$

where F_p and F_h are the \mathbf{h} -dependent gaps given by Eq. (4.8). Equation (4.37) implies that the influence of a free surface extends over the distance a particle-hole pair (with free energy $F_p + F_h$) can exist in thermal equilibrium at temperature T , as illustrated in Fig. 8.

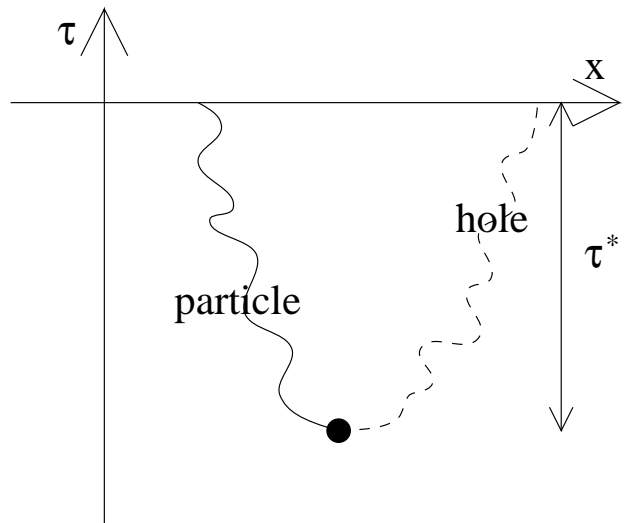


FIG. 8. The screening length τ^* of a transverse magnetic field is determined by the distance over which a particle-hole pair can exist in thermal equilibrium.

Away from the multicritical point, this particular “healing length” does *not* diverge near the superfluid phase: suppose, for example, that particles are the favored defects whose energy vanishes as we approach the transition. However, any particle excitation near the boundary must be accompanied by a hole, with a much higher free energy, yielding a finite healing length. Once we cross the transition into the flux liquid or “superfluid” phase, the free energy per unit length of extra particles becomes negative. Only then can it extend across the whole length of the sample, and no longer requires an accompanying vacancy.

For penetration at surfaces in other directions, we expect (although we have not done explicit calculations) that the magnetic field falls off exponentially with a decay length of

$$\tau^* = \frac{k_B T}{F(\theta, \phi) + F(\pi - \theta, \phi + \pi)}, \quad (4.38)$$

where (θ, ϕ) is the angle of the normal to the surface. Again, this will not diverge unless $c_\tau = \mathbf{c}_h = 0$.

V. SUPERFLUID PHASE

To study the superfluid phase, we must include quartic powers of $|\psi|$ in the action. Near the transition, the truncation (3.11) should be an adequate approximation, because other terms, such as $|\psi|^6$ and gradient operators combined with $\psi^* \psi^* \psi \psi$, are irrelevant variables.

Note first that in the superfluid phase, *both* particles and holes are present in equilibrium, even away from the exceptional multicritical point. As illustrated in Fig. 9, $\langle \psi(\mathbf{r}, \tau) \rangle \sim e^{-F_+/k_B T}$, where F_+ is the free energy associated with creation of a vortex “head” or magnetic monopole at position (\mathbf{r}, τ) . Similarly, $\langle \psi^*(\mathbf{r}, \tau) \rangle \sim e^{-F_-/k_B T}$, where F_- is the free energy associated with creation of a vortex “tail” or magnetic antimonopole. [26] In the Mott insulator phase, these heads and tails are accompanied by long strings of (energetically unfavorable) particle or hole excitations, so F_+ and F_- diverge as the sample thickness $L \rightarrow \infty$. The presence of both particles and holes in the superfluid phase follows because F_+ and F_- are finite, i.e.,

$$\lim_{|\tau| \rightarrow \infty} \langle \psi(\mathbf{r}, \tau) \psi^*(\mathbf{r}, 0) \rangle = \langle \psi(\mathbf{r}, \tau) \rangle \langle \psi^*(\mathbf{r}, 0) \rangle \neq 0. \quad (5.1)$$

When $c \neq 0$ or $\mathbf{c}_h \neq \mathbf{0}$, we find more precisely that

$$\lim_{|\tau| \rightarrow \infty} \langle \psi(\mathbf{r}, \tau) \psi^*(\mathbf{r}, 0) \rangle = |\langle \psi \rangle|^2 \sim |r \ln r| \quad (5.2)$$

just above the transition. The explicit expression for the condensate fraction $n_0 = |\langle \psi \rangle|^2$ is given in Appendix C. Thus both particles and holes will proliferate, even when only one of their energies vanishes at the transition, similar to results found for vacancies and interstitials at the supersolid transition by Frey *et al.* for supersolids [21], and as confirmed via the decoupling method of Appendix A. The ratio of particles to holes in the superfluid phase is more difficult to compute, and we rely on the decoupling method of Appendix A for a mean field estimate of this quantity. More generally, we expect that the probability of an m -fold particle or hole behaves as

$$\begin{aligned} \lim_{|\tau| \rightarrow \infty} \langle [\psi(x_i, \tau)]^m [\psi^*(x_i, 0)]^m \rangle \\ \sim \langle [\psi^*(x_i, \tau)]^m \rangle \langle [\psi(x_i, 0)]^m \rangle \\ \sim (|r \ln r|)^m, \end{aligned} \quad (5.3)$$

which has logarithmic corrections to the mean field results obtained in the decoupling approximation of Appendix A.

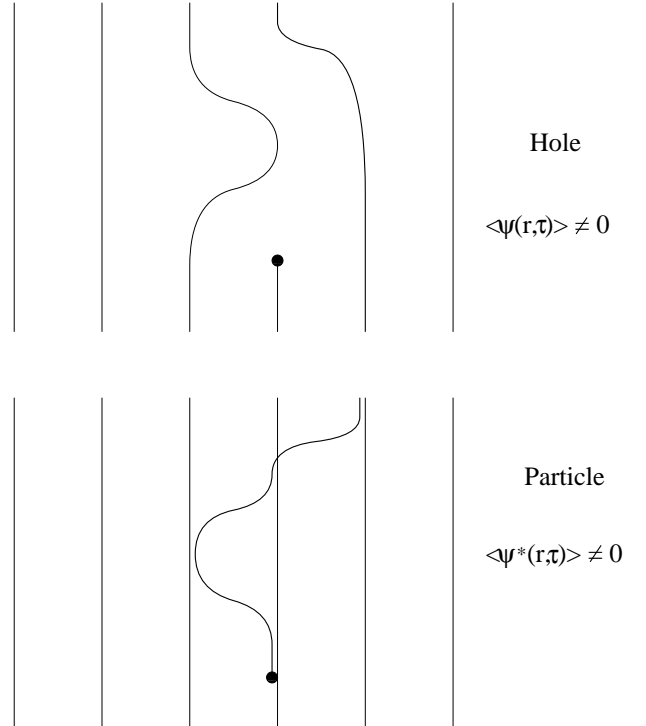


FIG. 9. Vortex “head” and “tail” excitations (monopoles) associated with $\langle \psi \rangle$ and $\langle \psi^* \rangle$. The corresponding free energies F_+ and F_- are finite in the superfluid phase, leading to $\langle \psi \rangle \neq 0$ and $\langle \psi^* \rangle \neq 0$, while in the Mott insulator phase there is a free energy cost *per unit length*, giving rise to $\langle \psi \rangle = \langle \psi^* \rangle = 0$ as $L_z \rightarrow \infty$.

A. Magnetic field penetration

Once in the superfluid phase, the magnetic field \mathbf{B} deviates from its frozen Mott insulator value $\mathbf{B}_0 = (n\phi_0/a_0^2)\hat{\mathbf{z}}$, unless the parameters are tuned to the multicritical point. Let $\delta\mathbf{B} = \mathbf{B} - \mathbf{B}_0$. We show explicitly that the excess magnetic field $\delta\mathbf{B}$ is determined by the angle that which tilted particles and holes enter at the transition.

The calculation of the magnetic field appears in Appendix E. The excess field (to lowest order in the condensate fraction) is given by

$$\delta\mathbf{B} = \phi_0 \mathbf{v} \frac{|r \ln r|}{16\pi D} \quad (5.4)$$

as $r \rightarrow 0$, where \mathbf{v} is defined in Eq. (3.16) and D is given in Eq. (C2). This adds further support to our claim that the transition is characterized by the penetration of “tilted defects,” as the excess magnetic field is indeed in the direction of these putative defects. Note that the magnitude of this excess field has the same dependence on the distance from the Mott insulator phase as it does in the pure case near the Meissner phase at H_{c1} . [3]

B. Excitation spectrum

We now discuss the spectrum of excitations in the superfluid phase. In the superfluid or entangled flux liquid phase, $\langle \psi(\mathbf{r}, \tau) \psi^*(\mathbf{0}, 0) \rangle$ exhibits long range order, as was discussed at the beginning of this section. Here, we discuss the flux lines themselves, and focus on correlations in the local vortex density

$$\hat{n}_i(\tau) = \hat{a}_i^\dagger(\tau) \hat{a}_i(\tau), \quad (5.5)$$

which are controlled by the excitation spectrum of the equivalent quantum superfluid. [3] Specifically, we expect that the spatial Fourier transform $\hat{n}(\mathbf{k}, \tau)$ of the density has the correlation

$$S(\mathbf{k}, \tau) \equiv \langle \hat{n}(\mathbf{k}, \tau) \hat{n}^*(\mathbf{k}, 0) \rangle \quad (5.6)$$

$$\sim S(\mathbf{k}, \tau = 0) \exp[-\epsilon_B(\mathbf{k})\tau/k_B T] \quad (5.7)$$

in the $\tau \rightarrow \infty$ limit, where the decay in the imaginary time direction is controlled by the phonon-roton spectrum $\epsilon_B(\mathbf{k})$ of the superfluid. [27] Our interest here is to find the form of this spectrum when the magnetic field is tilted to make the problem non-Hermitian. We assume the tilt is large enough to destroy the transverse Meissner defect and apply the Bogoliubov approximation [28] to Eq. (1.1), which will be accurate deep in the superfluid phase. This approximation treats creation and annihilation operators in the zero momentum Fourier mode as c -numbers, and then neglects interactions between bosons that are both outside the condensate. After some straightforward calculations, we find that the excitation spectrum that enters Eq. (5.7) is

$$\epsilon_B(\mathbf{k}) = \sqrt{2Un_0\epsilon_R(\mathbf{k}) + \epsilon_R^2(\mathbf{k}) + i\epsilon_I(\mathbf{k})}, \quad (5.8)$$

where n_0 is the average vortex density,

$$\epsilon_R(\mathbf{k}) = 2t[\cosh h_x(1 - \cos k_x a_0) + \cosh h_y(1 - \cos k_y a_0)], \quad (5.9)$$

and

$$\epsilon_I(\mathbf{k}) = 2t[\sinh h_x \sin k_x a_0 + \sinh h_y \sin k_y a_0]. \quad (5.10)$$

The real part of the spectrum (5.9) reduces to the usual lattice Bogoliubov spectrum when $\mathbf{h} = \mathbf{0}$. The imaginary part can be understood by considering the limit of small \mathbf{k} , when Eq. (5.8) can be written

$$\epsilon_B(\mathbf{k}) = \sqrt{2Un_0\epsilon_R(\mathbf{k})} + i\mathbf{u}_h \cdot \mathbf{k}, \quad (5.11)$$

where

$$\mathbf{u}_h = 2a_0 t(\sinh h_x, \sinh h_y) \quad (5.12)$$

is parallel to the tilt direction \mathbf{c}_h defined in Eq. (3.13). Equation (5.12) is just the famous Landau formula for excitations in a moving superfluid, [28] generalized to imaginary time. The imaginary part is required here to describe the drift of the entangled vortex lines relative to the column direction. This complex spectrum is similar to the spectrum of eigenvalues found for superfluid columnar in positions in the non-interacting case. [14,17].

ACKNOWLEDGMENTS

This research was supported primarily by the Harvard Materials Research Science and Engineering Laboratory through Grant No. DMR94-00396 and by the National Science Foundation through Grant No. DMR97-14725. One of us (R.A.L.) acknowledges support from the U.S. Office of Naval Research.

APPENDIX A: MEAN FIELD DECOUPLING

Following Sheshadri *et al.* [22] we make the decoupling approximation

$$\hat{a}_i^\dagger \hat{a}_j \approx \langle \hat{a}_i^\dagger \rangle \hat{a}_j + \hat{a}_i^\dagger \langle \hat{a}_j \rangle - \langle \hat{a}_i^\dagger \rangle \langle \hat{a}_j \rangle, \quad (A1)$$

so that the Hamiltonian (1.1) takes the form $\hat{\mathcal{H}} = \sum_i \hat{\mathcal{H}}_i$, with

$$\hat{\mathcal{H}}_i = \frac{U}{2} \hat{n}_i(\hat{n}_i - 1) - \mu \hat{n}_i - t^*[\psi \hat{a}_i^\dagger + \psi^* \hat{a}_j - |\psi|^2], \quad (A2)$$

and where the order parameter is $\psi = \langle \hat{a}_i \rangle$. The effective hopping strength t^* is given by

$$t^* = 2t(\cosh h_x + \cosh h_y). \quad (A3)$$

Since the sites are now decoupled in Eq. (A2), we focus on a single site, and drop the index i . We expand the ground state wave function of the site $|\Phi\rangle$ in the occupation number basis:

$$|\Phi\rangle = \sum_{n=0}^{\infty} f(n)|n\rangle, \quad (A4)$$

where $\sum |f(n)|^2 = 1$ to insure proper normalization of $|\Phi\rangle$, and $|f(n)|^2$ is the probability of finding n particles on a site. Then

$$\psi = \langle \hat{a}_i \rangle = \sum_{n=0}^{\infty} \sqrt{n+1} f^*(n) f(n+1), \quad (A5)$$

$$\psi^* = \langle \hat{a}_i^\dagger \rangle = \sum_{n=0}^{\infty} \sqrt{n+1} f(n) f^*(n+1), \quad (A6)$$

and

$$E = \langle \hat{\mathcal{H}} \rangle = \sum_{n=0}^{\infty} \left(\frac{U}{2} n(n-1) - \mu n \right) |f(n)|^2 - t^* |\psi|^2. \quad (A7)$$

For any fixed set of magnitudes $\{|f(n)|\}$ we can maximize $|\psi|$, and hence minimize E , by equating all the phases of the $f(n)$. So without loss of generality we assume that all $f(n)$ are real in the ground state wave function.

In the Mott insulator phase with n flux lines per site, we expect $f(n') = \delta_{n,n'}$, and it follows from Eq. (A5) that the order parameter $\psi = 0$. In the superfluid phase, $f(n')$ will in general be nonzero for all nonnegative integers n' ; however, near the transition, we expect defects with either $n+1$ or $n-1$ flux lines per sites to dominate. Hence, we neglect all other types of defects and write

$$f(n') = \begin{cases} \sqrt{\alpha} & \text{if } n' = n+1 \\ \sqrt{\beta} & \text{if } n' = n-1 \\ \sqrt{1-\alpha-\beta} & \text{if } n' = n \\ 0 & \text{otherwise,} \end{cases} \quad (\text{A8})$$

where α and β are variational parameters. If we reexpress α and β as

$$\alpha = \epsilon(1 + \omega), \quad (\text{A9})$$

$$\beta = \epsilon(1 - \omega), \quad (\text{A10})$$

then ϵ is the average number of particles *and* holes ($\epsilon \ll 1$ near the transition) and ω is the particle-hole asymmetry. Upon expanding Eq. (A7) to linear order in ϵ , we obtain

$$E = \epsilon[(E_p + E_h) + \omega(E_p - E_h) - t^*(\sqrt{n+1}\sqrt{1+\omega} + \sqrt{n}\sqrt{1-\omega})^2], \quad (\text{A11})$$

with E_p and E_h given by Eq. (3.14) and Eq. (3.15). By minimizing the bracketed term with respect to ω , and equating the result to zero, we find a transition from the Mott insulator to the superfluid in agreement with the Hubbard-Stratanovich result (4.3). The particle-hole asymmetry is given by

$$\omega = \frac{\mu - \mu_0}{\sqrt{(\mu - \mu_0)^2 + n(n+1)(t^*)^2}}, \quad (\text{A12})$$

where

$$\mu_0 = U(n - 1/2) - t^*/2. \quad (\text{A13})$$

We can also calculate the probability of finding more exotic defects, e.g., *two* extra particles on a site, as a check on the ansatz (A8). To this end, we minimize Eq. (A7) with respect to n' , with $n' \neq n$, subject to the constraint

$$f(n) = \sqrt{1 - \sum_{n' \neq n} [f(n')]^2} \quad (\text{A14})$$

and obtain

$$f(n') = \frac{t^*\psi[f(n+1)\sqrt{n'+1} + f(n-1)\sqrt{n'}]}{C_{n'} + t^*\psi\kappa} \quad (\text{A15})$$

for $n' \neq n$, with

$$\psi = \sum_{n'=0}^{\infty} \sqrt{n'+1}f(n')f(n'+1), \quad (\text{A16})$$

$$\kappa = \frac{[f(n+1)\sqrt{n+1} + f(n-1)\sqrt{n}]}{f(n)}, \quad (\text{A17})$$

and

$$C_{n'} = \frac{U}{2}(n' - n)^2 - [\mu - U(n - 1/2)](n' - n). \quad (\text{A18})$$

Although these equations are difficult to solve analytically, it is possible to extract the power law dependence of $f(n')$ on ϵ near the transition. Because $\psi \sim \kappa \sim \sqrt{\epsilon}$, we have a recursion relation

$$f(n') \sim \sqrt{\epsilon}[f(n'+1) + f(n'-1)], \quad (\text{A19})$$

with asymptotic solution

$$f(n') \sim \epsilon^{|n'-n|/2} \quad (\text{A20})$$

as $\epsilon \rightarrow 0$. Thus the fraction of sites with n' particles per site falls off like $\sim \epsilon^{|n'-n|}$ near the transition; the same result follows from the Hubbard-Stratanovich method.

APPENDIX B: EXPANSION OF EFFECTIVE ACTION

To expand the effective action of Eq. (3.6) in powers of ψ , first define the Fourier transform

$$\psi(\mathbf{k}, \omega) = \sum_i \int_0^L d\tau \psi_i(\tau) e^{-i(\mathbf{k} \cdot \mathbf{x}_i - \omega\tau)}, \quad (\text{B1})$$

$$\psi^*(\mathbf{k}, \omega) = \sum_i \int_0^L d\tau \psi_i^*(\tau) e^{i(\mathbf{k} \cdot \mathbf{x}_i - \omega\tau)}, \quad (\text{B2})$$

and

$$\widetilde{J}^{-1}(\mathbf{k}) = \sum_i (J^{-1})_{ij} e^{-i\mathbf{k} \cdot (\mathbf{x}_i - \mathbf{x}_j)}, \quad (\text{B3})$$

with periodic boundary conditions in all directions. Then, in the thermodynamic limit, the first term of Eq. (3.6) reads

$$\begin{aligned} & \beta \sum_{i,j} \int_0^L d\tau (J^{-1})_{ij} \psi_i^*(\tau) \psi_j(\tau) \\ & = \beta a_0^2 \int \frac{d^2 \mathbf{k} d\omega}{(2\pi)^3} |\psi(\mathbf{k}, \omega)|^2 \widetilde{J}^{-1}(\mathbf{k}), \end{aligned} \quad (\text{B4})$$

with

$$\widetilde{J}^{-1}(\mathbf{k}) = \frac{1}{2t \cos(k_x a_0 + i h_x) + \cos(k_y a_0 + i h_y)}. \quad (\text{B5})$$

We shall also need the second term of Eq. (3.6) expanded to quadratic order in ψ , namely

$$-\frac{\beta^2}{2} \sum_i \int_0^L d\tau_1 \int_0^L d\tau_2 \times \left[\psi_i(\tau_1) \psi_i^*(\tau_2) \left\langle T_\tau a_i^\dagger(\tau_1) a_i(\tau_2) \right\rangle_0 + \psi_i^*(\tau_1) \psi_i(\tau_2) \left\langle T_\tau a_i(\tau_1) a_i^\dagger(\tau_2) \right\rangle_0 \right], \quad (\text{B6})$$

where we have used the fact that $\hat{\mathcal{H}}_0$ conserves particle number.

Upon changing variables so that the earlier time is τ and the later time is $\tau + \delta\tau$, Eq. (B6) becomes

$$-\beta^2 \sum_i \int_0^L d\tau \int_0^{L/2} d\delta\tau \times \left[\psi_i(\tau + \delta\tau) \psi_i^*(\tau) \left\langle a_i^\dagger(\tau + \delta\tau) a_i(\tau) \right\rangle_0 + \psi_i^*(\tau + \delta\tau) \psi_i(\tau) \left\langle a_i(\tau + \delta\tau) a_i^\dagger(\tau) \right\rangle_0 \right]. \quad (\text{B7})$$

The expectation values in Eq. (B7) can be evaluated using the properties of the single site Hamiltonian (3.2), which is diagonal in the occupation number representation. For example,

$$\begin{aligned} & \left\langle a_i^\dagger(\tau + \delta\tau) a_i(\tau) \right\rangle_0 \\ &= \frac{\sum_{m=0}^{\infty} m e^{-\beta L E_m} e^{-\beta \delta\tau (E_{m-1} - E_m)}}{\sum_{m=0}^{\infty} e^{-\beta L E_m}}, \end{aligned} \quad (\text{B8})$$

where

$$E_m = \frac{U}{2} m(m-1) - \mu m. \quad (\text{B9})$$

In the limit $L \rightarrow \infty$, the sums are dominated by $m = n$ such that

$$(n-1) < \frac{\mu}{U} < n, \quad (\text{B10})$$

and we have

$$\left\langle a_i^\dagger(\tau + \delta\tau) a_i(\tau) \right\rangle_0 = n e^{-\beta \delta\tau E_h}, \quad (\text{B11})$$

$$\left\langle a_i(\tau + \delta\tau) a_i^\dagger(\tau) \right\rangle_0 = (n+1) e^{-\beta \delta\tau E_p}, \quad (\text{B12})$$

with E_h and E_p the hole and particle energies given by Eqs. (3.15) and (3.14).

We can now Fourier transform (B7), which upon combination with Eq. (B4) yields the action $S(\psi)$ that appears in Eq. (3.5) to second order in ψ :

$$S(\psi) \approx S_0(\psi) = \beta a_0^2 \int \frac{d^2 \mathbf{k} d\omega}{(2\pi)^3} |\psi(\mathbf{k}, \omega)|^2 \times \left[\widetilde{J^{-1}}(\mathbf{k}) - \frac{n}{E_h + i\omega k_B T} - \frac{n+1}{E_p - i\omega k_B T} \right]. \quad (\text{B13})$$

This quadratic approximation to the action is used to study the Mott insulator phase in Sec. IV. To determine the universality class of the Mott insulator/superfluid transition, we need the long-wavelength contributions (up to quadratic order in \mathbf{k} and ω) to the coefficient of $|\psi(\mathbf{k}, \omega)|^2$ and the zero-frequency part of $|\psi|^4$ in the expansion of Eq. (3.6). It is tedious, but straightforward, to find the result used in Sec. III, namely

$$S(\psi) \approx \beta a_0^2 \int \frac{d^2 \mathbf{k} d\omega}{(2\pi)^3} |\psi(\mathbf{k}, \omega)|^2 [r - i c_\mu \omega + i \mathbf{c}_h \cdot \mathbf{k} + c' \omega^2 + D_{ij} k_i k_j] + u \int d^2 \mathbf{r} d\tau |\psi(\mathbf{r}, \tau)|^4, \quad (\text{B14})$$

where

$$r = \frac{1}{2t} \frac{1}{\cosh h_x + \cosh h_y} - \frac{n}{E_h} - \frac{n+1}{E_p}, \quad (\text{B15})$$

$$c_\mu = k_B T \left(\frac{n+1}{E_p^2} - \frac{n}{E_h^2} \right), \quad (\text{B16})$$

$$\mathbf{c}_h = \frac{a_0}{2t} \frac{\hat{\mathbf{x}} \sinh h_x + \hat{\mathbf{y}} \sinh h_y}{[\cosh h_x + \cosh h_y]^2}, \quad (\text{B17})$$

and

$$c' = (k_B T)^2 \left(\frac{n+1}{E_p^3} + \frac{n}{E_h^3} \right). \quad (\text{B18})$$

The matrix D_{ij} reads

$$D = \begin{pmatrix} D_{xx} & D_{xy} \\ D_{xy} & D_{yy} \end{pmatrix}, \quad (\text{B19})$$

with

$$D_{xx} = \frac{a_0^2}{2t} \frac{1 + \cosh h_x \cosh h_y - \sinh^2 h_x}{(\cosh h_x + \cosh h_y)^3}, \quad (\text{B20})$$

$$D_{yy} = \frac{a_0^2}{2t} \frac{1 + \cosh h_x \cosh h_y - \sinh^2 h_y}{(\cosh h_x + \cosh h_y)^3}, \quad (\text{B21})$$

$$D_x = \frac{a_0^2}{2t} \frac{-2 \sinh h_x \sinh h_y}{(\cosh h_x + \cosh h_y)^3}, \quad (\text{B22})$$

while

$$u = \beta a_0^6 \left[\frac{(n+1)^2}{E_p^3} + \frac{n^2}{E_h^3} + \frac{n(n+1)(E_p + E_h)}{E_p^2 E_h^2} - \frac{(n+1)(n+2)}{E_p^2 E_{2p}} - \frac{n(n-1)}{E_h^2 E_{2h}} \right], \quad (\text{B23})$$

where E_{2p} and E_{2h} are the energies of ‘‘double particle’’ and ‘‘double hole’’ excitations respectively,

$$E_{2h} = 2\mu - (2n-3)U, \quad (\text{B24})$$

$$E_{2p} = (2n+1)U - 2\mu. \quad (\text{B25})$$

Note that $u > 0$ because $E_{2h} > 2E_h > 0$ and $E_{2p} > 2E_p > 0$.

APPENDIX C: RENORMALIZATION GROUP

We first review the renormalization group treatment of the action of Eq. (3.11) away from the multicritical point $c = \mathbf{c}_h = 0$. The analysis simplifies if we transform the axes of space and time so that the imaginary time axis is no longer the $\hat{\mathbf{z}}$ axis but coincides with the preferred direction of the particle or hole defects. We denote quantities in this rotated frame with a tilde. In this special coordinate frame, the term linear in $\tilde{\mathbf{k}}$ vanishes and the action takes the form

$$S(\psi) \approx \beta a_0^2 \int_{\tilde{\mathbf{k}}, \tilde{\omega}} |\psi(\tilde{\mathbf{k}}, \tilde{\omega})|^2 [r - iC\tilde{\omega} + D\tilde{k}^2] + u \int_{\tilde{\mathbf{r}}, \tilde{\tau}} |\psi(\tilde{\mathbf{r}}, \tilde{\tau})|^4, \quad (\text{C1})$$

where $C = |\mathbf{v}|$ from Eq. (3.16). In general the quadratic wave vector dependencies will take the form $D_{ij}\tilde{k}_i\tilde{k}_j$. However, we can rotate the spatial axes so that the matrix D_{ij} is diagonal, and then rescale the \tilde{x} and \tilde{y} axes (holding the area fixed) so that $D_{ij} = D\delta_{ij}$, giving the simpler expression above, with

$$D = \frac{a_0^2}{2t|\mathbf{v}|(\cosh h_x + \cosh h_y)^3} \times \left\{ \frac{c'}{2t}(\cosh h_x + \cosh h_y)(\cosh h_x \cosh h_y - 1) - c_\mu^2 \left[(\cosh^2 h_x + \cosh^2 h_y + 2)(\cosh h_x \cosh h_y - 2) + 2 \right] \right\}^{1/2}. \quad (\text{C2})$$

(It can be shown that the quantity in braces is always positive when $r \geq 0$.) Also, there should appear an $\tilde{\omega}^2$ piece and an $\tilde{\omega}\tilde{\mathbf{k}}$ piece. However, these terms can easily be shown to be irrelevant variables near the transition, similar to possible $\tilde{\mathbf{k}}$ and $\tilde{\omega}$ -dependent terms in the quadratic coupling. We add a high momentum cutoff, and thus allow only $|\tilde{\mathbf{k}}| < \Lambda$. Following, e.g., Ref. [24], we will integrate out degrees of freedom $\psi(\tilde{\mathbf{k}}, \tilde{\omega})$ with momenta in a shell $\Lambda b^{-1} < |\tilde{\mathbf{k}}| < \Lambda$ (and any $\tilde{\omega}$), and rescale positions by b and imaginary times by b^z to restore our original cutoff. We also rescale our fields by a factor b^ζ . In $d = 2$, u is marginally irrelevant at the Gaussian fixed point $u = 0$, allowing us to work perturbatively in u to lowest order. The most important diagrams for renormalizing r and u are shown in Fig. 10. In $d + 1$ dimensions, we set $z = 2$ and $\zeta = -d/2$ to keep C and D fixed. Upon letting $b = e^l$ with l infinitesimal, we obtain the renormalization group recursion relations in $d = 2$

$$\frac{dr}{dl} = 2r, \quad (\text{C3})$$

$$\frac{du}{dl} = -\frac{u^2}{4\pi CD\beta^2 a_0^4}. \quad (\text{C4})$$

Although u is irrelevant at the Gaussian fixed point, its slow decay to zero leads to logarithmic corrections to results calculated in the mean field approximation.

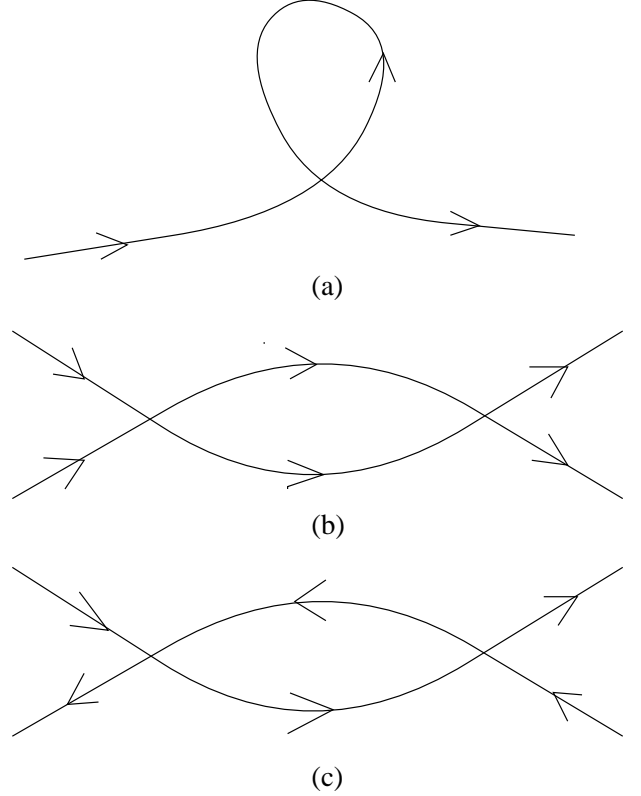


FIG. 10. (a) The most important diagram renormalizing r . (b) The most important diagram renormalizing u . (c) A diagram that vanishes identically.

To exhibit these logarithmic corrections, we first solve the recursion relation for u to get [with $u_0 = u(l=0)$]

$$u(l) = \frac{u_0}{1 + u_0 l / (4\pi CD\beta^2 a_0^4)}, \quad (\text{C5})$$

which behaves for large l like

$$u(l) \rightarrow \frac{4\pi CD\beta^2 a_0^4}{l}. \quad (\text{C6})$$

Consider now the condensate fraction

$$n_0 = |\langle \psi(\mathbf{r}, \tau) \rangle|^2 \quad (\text{C7})$$

right above the transition. We express n_0 as a function of the parameters in the Hamiltonian, and iterate them under the renormalization group. Then

$$n_0(r, C, D, u, \dots) \approx e^{2l\zeta} n_0(r(l), C(l), D(l), u(l), \dots). \quad (\text{C8})$$

We iterate until $r(l) \approx re^{2l} = 1$, i.e. $l = 1/2|\ln r|$, so that we are deep in the flux liquid or superfluid phase. Since $n_0 \approx \beta a_0^2 r(l)/2u(l)$ far from the transition, we find using $r(l) \approx re^{2l}$, $u(l) \approx 4\pi CD\beta^2 a_0^4/l$ that

$$|\langle\psi\rangle|^2 = n_0 = \frac{1}{16\pi CD\beta a_0^2} |r \ln r|, \quad (\text{C9})$$

which has logarithmic corrections from the naive result $n_0 \sim r$.

We now turn to the case where $c_\mu = \mathbf{c}_h = 0$, so we are at the multicritical point. Up to a simple rescaling of lengths, the action (3.11) is then isotropic in space and time, the dynamical exponent is $z = 1$, and the universality class is that of the three-dimensional XY model. As noted by Josephson [29], the superfluid density scales differently from the condensate fraction, with the condensate fraction behaving as

$$n_0 \sim (r_c - r)^{2\beta} \quad (\text{C10})$$

near the transition while the superfluid density behaves as

$$\rho_s \sim (r_c - r)^{2\beta - \nu\eta} \sim (r_c - r)^{(d-2)\nu}, \quad (\text{C11})$$

where $r_c - r$ is the distance from the transition. (The superfluid density is proportional to the inverse tilt modulus in the flux line system. [13,15]) We will have anomalous scaling for the superfluid density at the generic points of the phase boundary as well. Note that $\eta = 0$ since we are at the upper critical dimension of the generic H_{c1} transition, so the corrections are limited to the logarithmic terms.

1. Validity of the continuum limit

To explore the validity of taking the continuum limit, we add a new term into the action of Eq. (3.11) that represents a vestige of the periodic columnar array, namely

$$\delta S(\psi) = \beta \int d^2\mathbf{x} d\tau \delta r(\mathbf{x}) |\psi(\mathbf{x}, \tau)|^2, \quad (\text{C12})$$

where

$$\delta r(\mathbf{x}) = p \left[\cos\left(\frac{2\pi x}{a_0}\right) + \cos\left(\frac{2\pi y}{a_0}\right) \right]. \quad (\text{C13})$$

We then investigate how the addition of this term changes the renormalization group.

First we consider the case $\mathbf{h} = \mathbf{0}$, so that we do not have to rotate our coordinate system as in Eq. (C1). Then, in momentum space, the additional terms all involve terms such as $\psi(\mathbf{k}, \omega)\psi^*(\mathbf{k} + \mathbf{G}, \omega)$, where \mathbf{G} is a reciprocal lattice vector of the underlying square lattice. When we reach the point in our renormalization group procedure where $(2\pi/a_0)e^l = \Lambda$, all of the terms added in Eq. (C12) will be integrated out, leading only to finite

changes in the remaining coupling constants. Hence, the critical phenomena at the Mott insulator to superfluid transition will be unchanged by the addition of the periodic potential. Note that this argument applies both to the multicritical point and to the generic transition with $\mathbf{h} = \mathbf{0}$.

When $\mathbf{h} \neq \mathbf{0}$, we must rotate our coordinate system as in Eq. (C1). For most values of c_μ and \mathbf{c}_h , all of the terms in Eq. (C12) will still involve a jump in the momentum $\tilde{\mathbf{k}}$, so the argument above holds here as well. The exception is when the direction of the defects is perpendicular to the columns, i.e., $c_\mu = 0$. Then there will be terms in Eq. (C1) that involve a jump only in $\tilde{\omega}$, not in $\tilde{\mathbf{k}}$. We can rewrite these terms as

$$\delta S(\psi) = \beta a_0^2 \frac{p}{2} \int \frac{d^2\tilde{\mathbf{k}} d\tilde{\omega}}{(2\pi)^3} \psi(\tilde{\mathbf{k}}, \tilde{\omega}) \times \left[\psi^*(\tilde{\mathbf{k}}, \tilde{\omega} + \Delta) + \psi^*(\tilde{\mathbf{k}}, \tilde{\omega} - \Delta) \right], \quad (\text{C14})$$

where the initial value of Δ is $2\pi/a_0$.

We now investigate how the parameters p and Δ behave under the renormalization group. The diagrams renormalizing r , p , and u to one loop order are shown in Fig. 11. Note that all diagrams contributing to the renormalization of p in this approximation vanish identically, as do all of the extra diagrams that renormalize r . This vanishing persists to all orders in perturbation theory, because any diagram that contains a loop (of more than one propagator) with all the arrows pointing in the same direction, as illustrated in Figs. 10(c), 11(a), and 11(b), must vanish identically. Moreover, all diagrams renormalizing a propagator that contain any p -vertex must contain at least one such loop. Therefore, the zero-loop recursion relation for p is accurate to all orders in perturbation theory, yielding:

$$\frac{dp}{dl} = 2p, \quad (\text{C15})$$

$$\frac{d\Delta}{dl} = 2\Delta. \quad (\text{C16})$$

The recursion relation for r remains as given by Eq. (C3), accurate to one loop order. The recursion relation for u , however, has additional nonvanishing terms at one loop order, proportional to $u^2(p/\Delta)^{2n}$, for n a positive integer. (There are also terms with extra powers of Δ in the denominator, but those vanish in the large l limit.) Since p/Δ is independent of l , only the constant in Eq. (C4) is changed; the structure of the equations remains the same. In other words, we expect that, aside from prefactors, the results of our renormalization group calculations will be unchanged by the addition of a periodic potential. Therefore we can safely neglect terms with the periodicity of the columnar pins in our continuum description of the Mott insulator to superfluid transition.

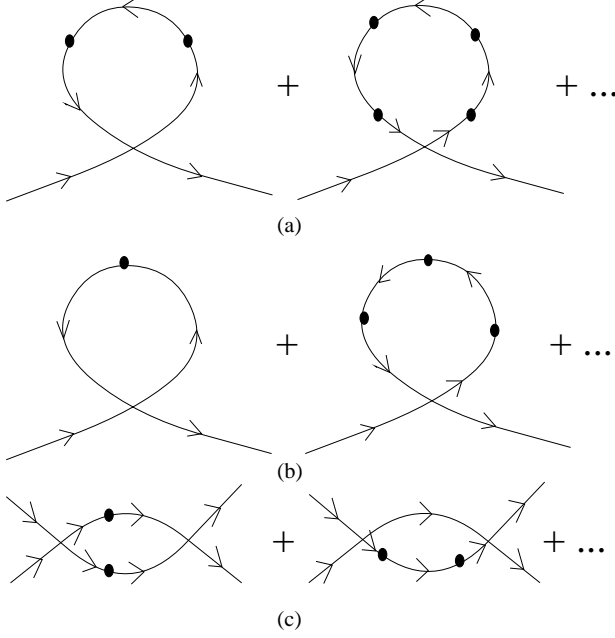


FIG. 11. (a) The diagrams involving factors of p that renormalize r . The dots are “interaction” vertices, with the interaction as given in Eq. (C14). The diagrams all vanish identically. (b) The diagrams renormalizing p . These also vanish identically. (c) Nontrivial diagrams involving factors of p that renormalize u .

APPENDIX D: FINITE SIZE EFFECT

In this appendix we examine a particular type of free surface effect, by showing that

$$\langle \hat{\mathcal{H}}_1 \rangle_\tau - \langle \hat{\mathcal{H}}_1 \rangle_{\tau=\infty} \sim e^{-\tau/\tau^*}, \quad (\text{D1})$$

where $\langle \hat{\mathcal{H}}_1 \rangle_\tau$ is defined in Eq. (4.34).

In the interaction representation, Eq. (4.34) takes the form

$$\langle \hat{\mathcal{H}}_1 \rangle_\tau = \frac{\mathcal{Z}_0}{\mathcal{Z}} \left\langle T_\tau \exp \left[-\beta \int_\tau^L d\tau' \hat{\mathcal{H}}_1(\tau') \right] \hat{\mathcal{H}}_1(\tau) \times T_\tau \exp \left[-\beta \int_0^\tau d\tau' \hat{\mathcal{H}}_1(\tau') \right] \right\rangle_0, \quad (\text{D2})$$

where

$$\mathcal{Z}_0 = \langle \psi_f | e^{-\beta L \hat{\mathcal{H}}_0} | \psi_i \rangle, \quad (\text{D3})$$

$$\langle \bullet \rangle_0 = \langle \psi_f | \bullet e^{-\beta L \hat{\mathcal{H}}_0} | \psi_i \rangle, \quad (\text{D4})$$

and

$$\mathcal{Z} = \left\langle T_\tau \exp \left[-\beta \int_0^L d\tau' \hat{\mathcal{H}}_1(\tau') \right] \right\rangle_0. \quad (\text{D5})$$

If we now define a composite partition function

$$\mathcal{Z}(\tau_1, \tau_2) = \left\langle T_\tau \exp \left[-\beta \int_{\tau_2}^L d\tau' \hat{\mathcal{H}}_1(\tau') \right] \times T_\tau \exp \left[-\beta \int_0^{\tau_1} d\tau' \hat{\mathcal{H}}_1(\tau') \right] \right\rangle_0, \quad (\text{D6})$$

then

$$\langle \hat{\mathcal{H}}_1 \rangle_\tau = -\frac{1}{\beta} \frac{\partial}{\partial \tau} \ln \mathcal{Z}(\tau, \tau_2) \Big|_{\tau=\tau_2}. \quad (\text{D7})$$

The Hubbard-Stratanovich transformation generalizes straightforwardly to $\mathcal{Z}(\tau_1, \tau_2)$, and leads via Eq. (D7) to

$$\langle \hat{\mathcal{H}}_1 \rangle_\tau = \langle K(\tau) \rangle_S, \quad (\text{D8})$$

where

$$K(\tau) = \sum_{i,j} (J^{-1})_{ij} \psi_i^*(\tau) \psi_j(\tau) - \sum_i \left\{ \left\langle T_\tau \exp \left[\beta \int_\tau^L d\tau' \hat{f}_i(\tau') \right] \hat{f}_i(\tau) \times T_\tau \exp \left[\beta \int_0^\tau d\tau' \hat{f}_i(\tau') \right] \right\rangle_0 \times \left\langle T_\tau \exp \left[\beta \int_0^L d\tau' \hat{f}_i(\tau') \right] \right\rangle_0^{-1} \right\}, \quad (\text{D9})$$

$$\hat{f}_i(\tau') = \psi_i(\tau') \hat{a}_i^\dagger(\tau') + \psi_i^*(\tau') \hat{a}_i(\tau'), \quad (\text{D10})$$

$$\langle \bullet \rangle_S = \frac{1}{\mathcal{Z}} \int \prod_i \mathcal{D}\psi_i(\tau) \mathcal{D}\psi_i^*(\tau) \bullet \exp[-S(\psi)], \quad (\text{D11})$$

and

$$S(\psi) = \beta \sum_{i,j} \int_0^L d\tau (J^{-1})_{ij} \psi_i^*(\tau) \psi_j(\tau) - \sum_i \ln \left\langle T_\tau \exp \left[\beta \int_0^L d\tau \{ \psi_i(\tau) \hat{a}_i^\dagger(\tau) + \psi_i^*(\tau) \hat{a}_i(\tau) \} \right] \right\rangle_0. \quad (\text{D12})$$

Although Eq. (D12) may appear to be identical to Eq. (3.6), the meaning of $\langle \bullet \rangle_0$ as well as the boundary conditions on ψ have changed. For “boson” boundary conditions, ψ was restricted to be periodic, i.e., $\psi_i(\tau=0) = \psi_i(\tau=\beta L)$. Following Ref. [3], we have inserted boundary conditions appropriate to vortices in a superconducting slab.

In the Mott insulator phase, it is again sufficient to expand the action to quadratic order in ψ , yielding

$$S(\psi) \approx S_0(\psi) + \delta S(\psi), \quad (\text{D13})$$

where $S_0(\psi)$ is given by Eq. (4.1) and $\delta S(\psi)$ is an extra piece due to the changed boundary conditions in a Mott insulator with n particles per site

$$\begin{aligned} \delta S(\psi) = & -na_0^2 \int \frac{d^2\mathbf{k}d\omega d\omega'}{(2\pi)^4} \psi(\mathbf{k}, \omega) \psi^*(\mathbf{k}, \omega') \\ & \times \left[\frac{e^{i\omega'\beta L}}{(E_h + i\omega k_B T)(E_h + i\omega' k_B T)} \right. \\ & \left. + \frac{e^{-i\omega\beta L}}{(E_p - i\omega k_B T)(E_p - i\omega' k_B T)} \right]. \quad (\text{D14}) \end{aligned}$$

We can now evaluate $\langle \hat{\mathcal{H}}_1 \rangle_\tau$ diagrammatically. Denote each $\delta S(\psi)$ with a cross. The diagrams that give the dominant contribution to $\langle \hat{\mathcal{H}}_1 \rangle_\tau - \langle \hat{\mathcal{H}}_1 \rangle_{\tau=\infty}$ as $\tau \rightarrow \infty$ are those in Fig. 12, i.e., those with two external lines and an even (but nonzero) number of crosses. In the limit $\tau \rightarrow \infty$ we find

$$\langle \hat{\mathcal{H}}_1 \rangle_\tau - \langle \hat{\mathcal{H}}_1 \rangle_{\tau=\infty} \sim e^{-(F_p + F_h)\tau/k_B T}, \quad (\text{D15})$$

which is Eq. (4.36).

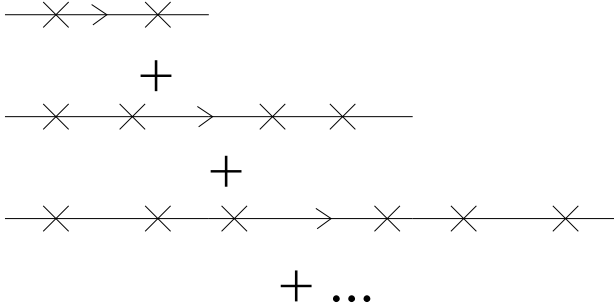


FIG. 12. The diagrams that give the dominant contribution to $\langle \hat{\mathcal{H}}_1 \rangle_\tau - \langle \hat{\mathcal{H}}_1 \rangle_\infty$ as $\tau \rightarrow \infty$. The crosses are free boundary insertions as given in Eq. (D14).

APPENDIX E: CALCULATION OF MAGNETIC FIELD IN SUPERFLUID PHASE

To calculate the magnetic field in the superfluid phase, we use the thermodynamic relation

$$\mathbf{B} = -4\pi \frac{\partial f}{\partial \mathbf{H}}, \quad (\text{E1})$$

where f is the free energy density $f = -(k_B T / Na_0^2 L_z) \ln \mathcal{Z}$ and the partition function \mathcal{Z} is given in Eq. (3.5) and Eq. (3.6).

We use Eq. (3.5) to evaluate \mathbf{B} . The piece that comes from \mathcal{Z}_0 is easily seen to be exactly the magnetic field

that we expect for a Mott insulator with occupation number n . The overall field is

$$\mathbf{B} = \frac{n\phi_0}{a_0^2} \hat{\mathbf{z}} - \frac{4\pi k_B T}{Na_0^2 L_z} \left\langle \frac{\partial S}{\partial \mathbf{H}} \right\rangle_S. \quad (\text{E2})$$

We first define

$$\delta \mathbf{B} \equiv \mathbf{B} - \frac{n\phi_0}{a_0^2} \hat{\mathbf{z}} \quad (\text{E3})$$

and

$$\delta \mathbf{H} \equiv \mathbf{H} - \frac{4\pi\epsilon_1}{\phi_0} \hat{\mathbf{z}}. \quad (\text{E4})$$

Then Eqs. (2.5) and (2.6) give

$$\delta \mathbf{H} = \frac{4\pi k_B T}{\phi_0} \left(\frac{\mathbf{h}}{a_0}, \beta\mu \right), \quad (\text{E5})$$

so that

$$\delta \mathbf{B} = -\frac{\phi_0}{Na_0^2 L_z} \left(a_0 \left\langle \frac{\partial S}{\partial \mathbf{h}} \right\rangle_S, k_B T \left\langle \frac{\partial S}{\partial \mu} \right\rangle_S \right). \quad (\text{E6})$$

Near the transition, we can use the action of Eq. (3.11) to evaluate the averages in Eq. (E6), obtaining

$$\begin{aligned} \delta \mathbf{B} \approx & \frac{\beta\phi_0}{NL_z} \int \frac{d^2\mathbf{k}d\omega}{(2\pi)^3} \langle |\psi(\mathbf{k}, \omega)|^2 \rangle \left[c_\mu \hat{\mathbf{z}} + \mathbf{c}_h \right. \\ & \left. + 2ic'\omega \hat{\mathbf{z}} - iD_{ij}(k_i \hat{e}_j + k_j \hat{e}_i) \right] \\ & - \frac{\phi_0 k_B T}{Na_0^2 L_z} \frac{\partial u}{\partial \mu} \hat{\mathbf{z}} \int d^2\mathbf{r}d\tau \langle |\psi(\mathbf{r}, \tau)|^4 \rangle + \dots, \quad (\text{E7}) \end{aligned}$$

where the omitted terms reflect contributions left out of Eq. (3.11). [Note that $\partial u / \partial \mu$ is proportional to the coefficient of the $\omega |\psi|^4$ term that would appear in Eq. (3.11).] To see which terms will yield the most important contributions, we transform the axes of space and imaginary time as in Appendix C. We have already determined the scaling of the coefficients under the action of the renormalization group, because they are the same coefficients as appear in the action. We discard those terms whose coefficients are irrelevant, and obtain

$$\delta \mathbf{B} = \frac{\beta\phi_0}{NL_z} \int \frac{d^2\tilde{\mathbf{k}}d\tilde{\omega}}{(2\pi)^3} \left\langle |\psi(\tilde{\mathbf{k}}, \tilde{\omega})|^2 \right\rangle \left[\mathbf{v} - 2iD\tilde{\mathbf{k}} \right], \quad (\text{E8})$$

where \mathbf{v} is given by Eq. (3.16). We then iterate the renormalization group until $|r(l)| = 1$, so that we are far from the transition, and can use mean field theory. If the flow begins on the Mott insulator side of the transition, then we will iterate until we are deep in the Mott insulator phase and Eq. (E8) vanishes. If the flow begins on the superfluid side of the transition, then deep in the superfluid phase we can set $|\psi(\tilde{\mathbf{r}}, \tilde{\tau})| \approx \sqrt{\beta a_0^2 r(l) / 2u(l)}$, independent of space and imaginary time. This yields

$$\delta \mathbf{B} \approx \phi_0 \beta a_0^2 \mathbf{v} \langle |\psi|^2 \rangle. \quad (\text{E9})$$

We therefore identify $\hat{\mathbf{v}}$ with the average direction of the tilted defects, and $n = \beta a_0^2 |\mathbf{v}| \langle |\psi|^2 \rangle$ with their density. Performing a scaling analysis similar to what was done for the condensate fraction n_0 in Appendix C, we obtain (away from the multicritical point)

$$\delta \mathbf{B} \approx \phi_0 \hat{\mathbf{v}} \frac{|r \ln r|}{16\pi D} \quad (\text{E10})$$

using $C = |\mathbf{v}|$ and with D given in Eq. (C2). At the multicritical point, $\mathbf{v} = 0$, so Eq. (E9) gives $\delta \mathbf{B} = 0$ near the transition.

-
- [1] G. Blatter, M. V. Feigel'man, V. B. Geshkenbein, A. I. Larkin, and V. M. Vinokur, *Rev. Mod. Phys.* **66**, 1125 (1994).
- [2] E. Brézin, D. R. Nelson, and A. Thiaville, *Phys. Rev. B* **31**, 7124 (1985).
- [3] D. R. Nelson, *Phys. Rev. Lett.* **60**, 1973 (1988); D. R. Nelson and H. S. Seung, *Phys. Rev. B* **39**, 9153 (1989).
- [4] R. C. Budhani, M. Suenaga, and S. H. Liou, *Phys. Rev. Lett.* **69**, 3816 (1992).
- [5] M. Konczykowski, F. Rullier-Albenque, E. R. Yacoby, A. Shaulov, Y. Yeshurun, and P. Lejay, *Phys. Rev. B* **44**, 7167 (1991).
- [6] L. Civale, A. D. Marwick, T. K. Worthington, M. A. Kirk, J. R. Thompson, L. Krusin-Elbaum, Y. Sun, J. R. Clem, and F. Holtzberg, *Phys. Rev. Lett.* **67**, 648 (1991).
- [7] W. Gerhäuser, G. Ries, H. W. Neumüller, W. Schmidt, O. Eibl, G. Saemann-Ischenko, and S. Klaumünzer, *Phys. Rev. Lett.* **68**, 879 (1992).
- [8] V. Hardy, D. Groult, M. Hervieu, J. Provost, B. Raveau, and S. Bouffard, *Nucl. Instrum. Methods Phys. Res. B* **54**, 472 (1991).
- [9] L. D. Cooley, P. J. Lee, and D. C. Larbalestier, *Appl. Phys. Lett.* **64**, 1298 (1994).
- [10] P. Lobotka, I. Vávra, R. Senderák, D. Machajdík, M. Jergel, Š. Gaži, E. Rosseel, M. Baert, Y. Bruynseraede, M. Forsthuber, and G. Hilscher, *Physica C* **229**, 231 (1994); M. Baert, V. V. Metlushko, R. Jonckheere, V. V. Moshchalkov, and Y. Bruynseraede, *Europhys. Lett.* **29**, 157 (1995); *Phys. Rev. Lett.* **74**, 3269 (1995).
- [11] Y.-H. Li and S. Teitel, *Phys. Rev. Lett.* **66**, 3301 (1991); *Phys. Rev. B* **45**, 5718 (1992); *ibid.* **47**, 359 (1993); *ibid.* **49**, 4136 (1994).
- [12] A. K. Nguyen, A. Sudbø, and R. E. Hetzel, *Phys. Rev. Lett.* **77**, 1592 (1996); M. J. P. Gingras and D. A. Huse, *Phys. Rev. B* **53**, 15193 (1996); G. Carneiro, *ibid.* **53**, 11837 (1996); G. Carneiro, *Phys. Rev. Lett.* **75**, 521 (1995); S. E. Shafranjuk, M. Tachiki, and T. Yamashita, *Phys. Rev. B* **55**, 8425 (1997); I.-J. Hwang and D. Stroud, *ibid.* **54**, 14978 (1996); I.-J. Hwang, R. Šášik, and D. Stroud, *ibid.* **54**, 12010 (1996); S. Ryu and D. Stroud, *ibid.* **54**, 1320 (1996).
- [13] D. R. Nelson and V. M. Vinokur, *Phys. Rev. B* **48**, 13060 (1993).
- [14] N. Hatano and D. R. Nelson, *Phys. Rev. Lett.* **77**, 570 (1996); N. Hatano and D. R. Nelson, *Phys. Rev. B* **56**, 8651 (1997).
- [15] U. C. Täuber and D. R. Nelson, *Phys. Rep.* **289**, 157 (1997).
- [16] M. P. A. Fisher, P. B. Weichman, G. Grinstein, and D. S. Fisher, *Phys. Rev. B* **40**, 546 (1989).
- [17] See, e.g., K. B. Efetov, *Phys. Rev. Lett.* **79**, 491 (1997); P. W. Brouwer, P. G. Silvestrov, and C. W. J. Beenakker, *Phys. Rev. B* **56**, R4333 (1997); E. Brézin and A. Zee, *cond-mat/9708029*; J. Feinberg and A. Zee, *cond-mat/9710040*; I. Y. Goldsheid and B. A. Khoruzhenko, *Phys. Rev. Lett.* **80**, 2897 (1998).
- [18] If the single particle eigenfunctions of Eq. (1.1) with $U = 0$ are indexed by a Bloch wave vector \mathbf{k} , then *all* vortex lines in the noninteracting model will reside in the $\mathbf{k} = \mathbf{0}$ state for sufficiently thick samples, as in Bose-Einstein condensation.
- [19] For a similar discussion of vortex wondering due to intrinsic pinning in cuprates by CuO_2 planes with fields perpendicular to the c -axis see L. Balents and D. R. Nelson, *Phys. Rev. B* **52**, 12951 (1995).
- [20] We concentrate here on a simplified “tight binding” model which assumes the energy cost of double occupancy is less than that required for one vortex to wander in the interstitial region. The energy cost of multiple occupancy could be lowered into this regime by increasing cross sectional area of the defects.
- [21] E. Frey, D. R. Nelson, and D. S. Fisher, *Phys. Rev. B* **49**, 9723 (1994).
- [22] K. Sheshadri, H. R. Krishnamurthy, R. Pandit, and T. V. Ramakrishnan, *Europhys. Lett.* **22**, 257 (1993).
- [23] S. Doniach, *Phys. Rev. B* **24**, 5063 (1981).
- [24] D. S. Fisher and P. C. Hohenberg, *Phys. Rev. B* **37**, 4936 (1988). For a direct diagrammatic approach, see V. N. Popov, *Functional Integrals and Collective Excitations* (Cambridge University Press, New York, 1987).
- [25] D. S. Fisher, M. P. A. Fisher, and D. A. Huse, *Phys. Rev. B* **43**, 130 (1991).
- [26] D. R. Nelson, in *Phenomenology and Applications of High Temperature Superconductors*, edited by K. S. Bedell, M. Inui, D. E. Meltzer, J. R. Schrieffer, and S. Doniach (Addison-Wesley, New York, 1991).
- [27] For an experimental measurement of this spectrum without columnar defects or tilt, see S. Yoon, Z. Yao, H. Dai, and C. M. Lieber, *Science* **270**, 270 (1995).
- [28] N. Bogoliubov, *J. Phys. USSR* **11**, 23 (1947); E. M. Lifshitz and L. P. Pitaevskii, *Statistical Physics, Part 2* (Pergamon Press, New York, 1980).
- [29] B. D. Josephson, *Phys. Lett.* **21**, 608 (1966).